

Uncertainty-Calibrated Test-Time Model Adaptation without Forgetting

Mingkui Tan*, Guohao Chen*, Jiaxiang Wu, Yifan Zhang, Yaofo Chen, Peilin Zhao, and Shuaicheng Niu†

Abstract—Test-time adaptation (TTA) seeks to tackle potential distribution shifts between training and testing data by adapting a given model w.r.t. any testing sample. This task is particularly important when the test environment changes frequently. Although some recent attempts have been made to handle this task, we still face two key challenges: 1) prior methods have to perform backpropagation for each test sample, resulting in unbearable optimization costs to many applications; 2) while existing TTA solutions can significantly improve the test performance on out-of-distribution data, they often suffer from severe performance degradation on in-distribution data after TTA (known as catastrophic forgetting). To this end, we have proposed an Efficient Anti-Forgetting Test-Time Adaptation (EATA) method which develops an active sample selection criterion to identify reliable and non-redundant samples for test-time entropy minimization. To alleviate forgetting, EATA introduces a Fisher regularizer estimated from test samples to constrain important model parameters from drastic changes. However, in EATA, the adopted entropy loss consistently assigns higher confidence to predictions even when the samples are underlying uncertain, leading to overconfident predictions that underestimate the data uncertainty. To tackle this, we further propose EATA with Calibration (EATA-C) to separately exploit the reducible model uncertainty and the inherent data uncertainty for calibrated TTA. Specifically, we compare the divergence between predictions from the full network and its sub-networks to measure the reducible model uncertainty, on which we propose a test-time uncertainty reduction strategy with divergence minimization loss to encourage consistent predictions instead of overconfident ones. To further re-calibrate predicting confidence on different samples, we utilize the disagreement among predicted labels as an indicator of the data uncertainty. Based on this, we devise a min-max entropy regularization to selectively increase and decrease predicting confidence for confidence re-calibration. Note that EATA-C and EATA are different on the adaptation objective, while EATA-C still benefits from the active sample selection criterion and anti-forgetting Fisher regularization proposed in EATA. Extensive experiments on image classification and semantic segmentation verify the effectiveness of our proposed methods.

Index Terms—Out-of-Distribution Generalization, Test-Time Adaptation, Calibration, Catastrophic, Forgetting, Robustness.

1 INTRODUCTION

DEEP neural networks (DNNs) have achieved excellent performance in many challenging tasks, including image classification [1], video recognition [2], [3], [4], [5], and many other areas [6], [7], [8]. One prerequisite behind the success of DNNs is that the test samples are drawn from the same distribution as the training data, which, however, is often violated in many real-world applications. In practice, test samples may encounter natural variations or corruptions (also called *distribution shift*), such as changes in lighting resulting from weather changes and unexpected noises resulting from sensor degradation [9], [10]. Unfortunately, models are often very sensitive to such distribution shifts and suffer severe performance degradation.

Recently, several attempts [11], [12], [13], [14], [15], [16] have been proposed to handle the distribution shifts by online adapting a model at test time (called *test-time adaptation*). Test-time training (TTT) [11] first proposes this pipeline. Given a test sample,

TTT first fine-tunes the model via rotation classification [17] and then makes a prediction using the updated model. Without the need of training an additional self-supervised head, Tent [12] and MEMO [14] further leverage the prediction entropy for test-time adaptation, in which the adaptation only involves test samples and a trained model. Although recent test-time adaptation methods are effective at handling test shifts, in real-world applications, they still suffer from the following limitations.

Latency Constraints. Since TTA adapts a given model during inference, the adaptation efficiency is paramount in scenarios where latency is a critical factor. Previous methods, such as Test-Time Training (TTT) [11] and MEMO [14], often require performing multiple backward propagations for each test sample. However, the computation-intensive nature of backward propagation renders these methods impractical in situations where low latency is non-negotiable or computational resources are limited.

Forgetting on In-Distribution Samples. Prior methods often focus on boosting the performance of a trained model on out-of-distribution (OOD) test samples, ignoring that the model after test-time adaptation suffers a severe performance degradation (named *forgetting*) on in-distribution (ID) test samples (see Figure 3). An eligible test-time adaptation approach should perform well on both OOD and ID test samples simultaneously, since test samples often come from both ID and OOD domains in real-world applications.

Over-Confident Predictions. Existing methods like Tent [12] and SAR [18] primarily focus on reducing the model’s prediction uncertainty through unsupervised prediction entropy minimization, which enhances the model’s predicting confidence, thereby learning

- Mingkui Tan, Guohao Chen, and Yaofo Chen are with the School of Software Engineering, South China University of Technology. Mingkui Tan and Guohao Chen are also with Pazhou Laboratory, Guangzhou, China. Email: mingkuitan@scut.edu.cn, {secasper, sechenyaofo}@mail.scut.edu.cn.
- Jiaxiang Wu is with XVERSE, China. The majority of this work was conducted while at Tencent AI Lab. Email: jiaxiang.wu.90@gmail.com.
- Yifan Zhang is with the School of Computing, National University of Singapore. Email: yifan.zhang@u.nus.edu.
- Peilin Zhao is with Tencent AI Lab, China. Email: masonzhao@tencent.com.
- Shuaicheng Niu is with the School of Computer Science and Engineering, Nanyang Technological University, Singapore. Email: shuaicheng.niu@ntu.edu.sg.

* Authors contributed equally. † Corresponding author.

TABLE 1

Characteristics of problem settings that adapt a trained model to a potentially shifted test domain. ‘Offline’ adaptation assumes access to the entire source or target dataset, while ‘Online’ adaptation can predict a single or batch of incoming test samples immediately.

Setting	Source Data	Target Data	Training Loss	Testing Loss	Offline	Online	Source Acc.	Prediction Uncertainty
Fine-tuning	\times	$\mathbf{x}^t, \mathbf{y}^t$	$\mathcal{L}(\mathbf{x}^t, \mathbf{y}^t)$	–	✓	\times	Not Considered	Not Considered
Continual learning	\times	$\mathbf{x}^t, \mathbf{y}^t$	$\mathcal{L}(\mathbf{x}^t, \mathbf{y}^t)$	–	✓	\times	Maintained	Not Considered
Unsupervised domain adaptation	$\mathbf{x}^s, \mathbf{y}^s$	\mathbf{x}^t	$\mathcal{L}(\mathbf{x}^s, \mathbf{y}^s) + \mathcal{L}(\mathbf{x}^t, \mathbf{y}^t)$	–	✓	\times	Maintained	Not Considered
Test-time training	$\mathbf{x}^s, \mathbf{y}^s$	\mathbf{x}^t	$\mathcal{L}(\mathbf{x}^s, \mathbf{y}^s) + \mathcal{L}(\mathbf{x}^t, \mathbf{y}^t)$	$\mathcal{L}(\mathbf{x}^t)$	\times	✓	Not Considered	Not Considered
Fully test-time adaptation (FTTA)	\times	\mathbf{x}^t	\times	$\mathcal{L}(\mathbf{x}^t)$	\times	✓	Not Considered	Not Considered
EATA (ours)	\times	\mathbf{x}^t	\times	$\mathcal{L}(\mathbf{x}^t)$	\times	✓	Maintained	Not Considered
EATA-C (ours)	\times	\mathbf{x}^t	\times	$\mathcal{L}(\mathbf{x}^t)$	\times	✓	Maintained	Calibrated

a decision boundary positioned in low-density sample regions [19], [20]. However, a critical oversight of these methods is their neglect of the irreducible data uncertainty inherent in test samples. They encourage highly certain predictions for all test samples even in cases of underlying data uncertainty or even if the prediction is wrong, leading to overly certain (or overconfident) predictions. This phenomenon is particularly concerning in high-risk applications [21], [22], posing potential safety risks.

To address the efficiency and forgetting issue, we have proposed an Efficient Anti-forgetting Test-time Adaptation (EATA) method consisting of a sample-efficient optimization strategy and a weight regularizer. EATA excludes unreliable samples characterized by high entropy values and redundant samples that are highly similar throughout the adaptation. In this case, we can reduce the total number of backward updates of test data streaming (improving efficiency) and enhance the model performance on OOD samples. Furthermore, EATA devises an anti-forgetting regularizer to prevent the important weights of the model from changing a lot during the adaptation, where the weights’ importance is measured based on Fisher information [23] via a small set of test samples. With this regularization, the model can continually adapt to OOD test samples without performance degradation on ID test samples.

To mitigate the over-confident issue, it is essential to differentiate between various origins of uncertainty in TTA, *i.e.*, reducible model uncertainty and inherent data uncertainty. Inspired by the human tendency to base predictions on *available knowledge* and *problem difficulty*, rather than defaulting to high certainty in unfamiliar situations, we propose to utilize the model uncertainty for calibrated uncertainty reduction and leverage the inherent data uncertainty to directly re-calibrate predicting confidence.

To this end, we further propose EATA with Calibration, namely EATA-C. To be specific, EATA-C estimates model uncertainty by measuring the divergence between predictions from the full network and its randomly sampled sub-networks. This allows for the reduction of model uncertainty by minimizing the divergence, promoting consistent rather than overconfident predictions during testing. Additionally, we develop a simple but effective indicator of data uncertainty based on the disagreement among predicted labels, which suggests whether a sample nears decision boundaries. Then, we devise an auxiliary min-max entropy regularizer to selectively lower confidence for inherently uncertain samples through an entropy maximization loss, while simultaneously boosting confidence for certain samples via an entropy minimization loss. EATA-C differs from EATA on the adaptation objective, while it still benefits from the active sample selection criterion and anti-forgetting Fisher regularization proposed in EATA. We summarize our main contributions as follows.

- We propose an Efficient Anti-forgetting Test-time Adaptation (EATA) method. Specifically, we develop an active sample identification scheme to filter out non-reliable and redundant test samples from model adaptation, thereby improving adaptation efficiency by reducing backward propagation. Moreover, we extend the label-dependent Fisher regularizer to test samples with pseudo label generation, which prevents drastic changes in important model weights and thus alleviates the issue of model forgetting on in-distribution test samples.
- We further propose EATA with Calibration (EATA-C), which decouples the model and data uncertainty to achieve confidence-calibrated TTA. Specifically, EATA-C estimates model uncertainty using the divergence between full network and sub-network predictions, incorporating a consistency loss to reduce this uncertainty without leading to overconfidence. For data uncertainty, EATA-C utilizes label prediction disagreements, employing min-max entropy regularization to selectively adjust prediction confidence for effective re-calibration.
- We demonstrate that our proposed EATA method improves both the performance and efficiency of test-time adaptation and also alleviates the long-neglected catastrophic forgetting issue, and EATA-C further achieves better performance and calibration without additional backward computations compared with EATA.

2 RELATED WORK

We divide the discussion on related works based on the different adaptation settings summarized in Table 1 and further review existing methods for model’s uncertainty calibration.

Test-Time Adaptation (TTA) aims to improve model accuracy on OOD test data through model adaptation with test samples, which has been successfully applied to various tasks, such as image classification [11], [12], image super-resolution [24], image captioning [25], object detection [26], video recognition [27], [28], *etc.* Existing test-time training methods, *e.g.*, TTT [11], TTT++ [13], TTT-MAE [29], and MT3 [30], jointly train a source model via both supervised and self-supervised objectives, and then adapt the model via self-supervised objective at test time. This pipeline, however, necessitates both self-supervised head and test data in adaptation, while training such self-supervised head can be computation-consuming [29]. To address this, some methods have been proposed to adapt a model with only test data, including batchnorm statistics adaptation [31], [32], [33], prediction consistency maximization over different augmentations [34], and classifier adjustment [35]. Specifically, Tent [12] updates the model to minimize the entropy of predictions at test time. MEMO [14] further augments test samples for marginal entropy minimization to enhance robustness. Our work also alleviates the dependency on

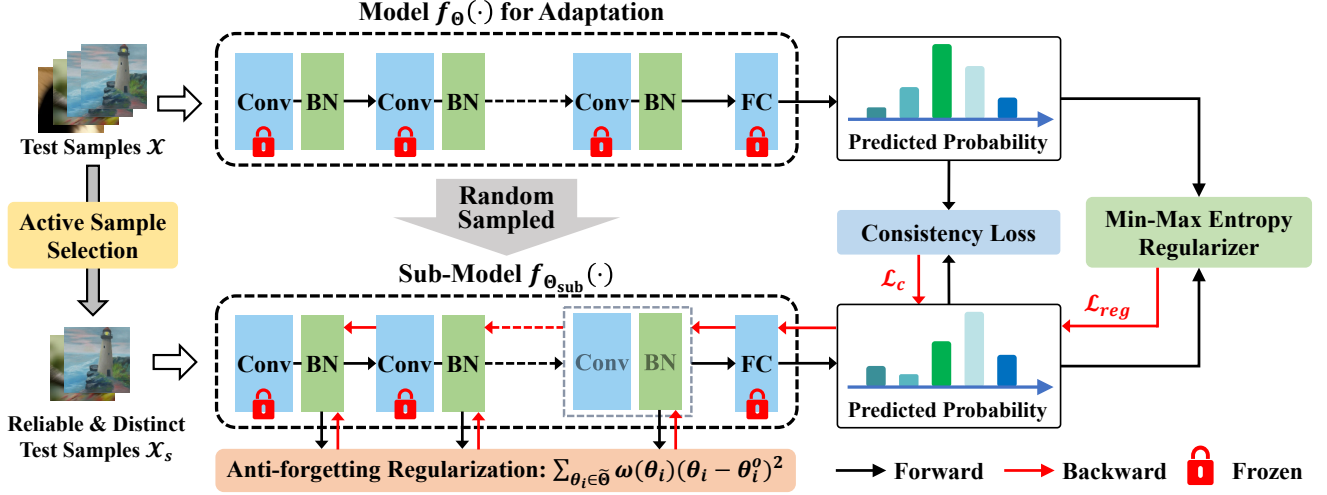


Fig. 1. An illustration of our proposed Efficient Anti-forgetting Test-time Adaptation with Calibration (EATA-C) method. During the test-time adaptation process, we update only the affine parameters of normalization layers in f_{Θ} and keep all other parameters frozen. Given a batch of incoming test samples $\mathcal{X} = \{\mathbf{x}_b\}_{b=1}^B$, we select the reliable and non-redundant ones \mathcal{X}_s with an active sample selection criterion to conduct model update, thereby enhancing adaptation efficiency. These samples are then used for calculating the proposed unidirectional consistency loss to minimize the model uncertainty. Additionally, we devise a min-max entropy regularizer for confidence re-calibration based on the data uncertainty of each sample. Lastly, we introduce an anti-forgetting regularizer which prevents the important model parameters in Θ from changing too much.

self-supervision heads and seeks to address the key limitations of prior works (*i.e.*, efficiency hurdle, catastrophic forgetting, and overconfidence) to make TTA more practical in real-world applications.

Continual Learning (CL) aims to help the model remember the essential concepts that have been learned previously, alleviating the catastrophic forgetting issue when learning a new task [23], [36], [37], [38], [39], [40]. In our work, we share the same motivation as CL and point out that test-time adaptation also suffers catastrophic forgetting (*i.e.*, performance degradation on ID test samples), which makes TTA approaches unstable to deploy. To conquer this, we propose a simple yet effective solution to maintain the model performance on ID test samples (by only using test data) and meanwhile improve the performance on OOD test samples.

Unsupervised Domain Adaptation (UDA). Conventional UDA tackles distribution shifts by jointly optimizing a source model on both labeled source data and unlabeled target data, such as devising a domain discriminator to learn domain-invariant features [41], [42], [43], [44]. To avoid access to source data, recently CPGA [45] generates feature prototypes for each category with pseudo-labeling. SHOT [46] learns a target-specific feature extractor by information maximization for representations alignment. Nevertheless, such methods optimize offline via multiple epochs and losses. In contrast, our method adapts in an online manner and selectively performs once backward propagation for one given target sample, which is more efficient during inference.

Uncertainty Calibration. A calibrated model refers to whose predicting confidence reflects the true likelihood of correctness. Post-training processing methods [47], [48], [49] re-calibrate a trained model by leveraging a labeled dataset within the target domain to estimate calibration error. In contrast, regularization-based methods [50], [51], [52], [53] introduce auxiliary objectives to improve calibration at the training phase. Recently, SB-ECE [54] proposes a differentiable estimation of calibration error as regularization to be jointly minimized. ESD [55] further reformulates the calibration objective in a class-wise manner to enhance calibration performance. Nevertheless, these methods necessitate labeled data

from the source or target domain, which limits their applicability. Unlike these methods, we seek to improve calibration with only access to unlabeled test data in an online manner in TTA context.

3 PROBLEM FORMULATION

Without loss of generality, let $P(\mathbf{x})$ be the distribution of training data $\{\mathbf{x}_i\}_{i=1}^N$ (namely $\mathbf{x}_i \sim P(\mathbf{x})$) and $f_{\Theta^o}(\mathbf{x})$ be a **base model** trained on labeled training data $\{(\mathbf{x}_i, y_i)\}_{i=1}^N$, where Θ^o denotes the model parameters. Due to the training process, the model $f_{\Theta^o}(\mathbf{x})$ tends to fit (or overfit) the training data. During the inference state, the model shall perform well for the in-distribution test data, namely $\mathbf{x} \sim P(\mathbf{x})$. However, in practice, due to possible distribution shifts between training and test data, we may encounter many out-of-distribution test samples, namely $\mathbf{x} \sim Q(\mathbf{x})$, where $Q(\mathbf{x}) \neq P(\mathbf{x})$. In this case, the prediction would be very unreliable and the performance is also very poor.

Test-time adaptation (TTA) [12], [14] aims at boosting the out-of-distribution prediction performance by doing model adaptation on test data only. Specifically, given a set of test samples $\{\mathbf{x}_j\}_{j=1}^M$, where $\mathbf{x}_j \sim Q(\mathbf{x})$ and $Q(\mathbf{x}) \neq P(\mathbf{x})$, one needs to adapt $f_{\Theta}(\mathbf{x})$ to improve the prediction performance on test data in any cases. To achieve this, existing methods often seek to update the model by minimizing some unsupervised objective defined on test samples:

$$\min_{\Theta} \mathcal{L}(\mathbf{x}; \Theta), \mathbf{x} \sim Q(\mathbf{x}), \quad (1)$$

where $\tilde{\Theta} \subseteq \Theta$ denotes the free model parameters that should be updated. In general, the test-time learning objective $\mathcal{L}(\cdot)$ can be formulated as an entropy minimization problem [12] or prediction consistency maximization over data augmentations [14], *etc.*

For existing TTA methods like TTT [11] and MEMO [14], during the test-time adaptation, we shall need to compute one round or even multiple rounds of backward computation for each sample, which is very time-consuming and also not favorable for latency-sensitive applications. Moreover, most methods assume that all the test samples are drawn from out-of-distribution (OOD). However, in practice, the test samples may come from both in-distribution

(ID) and OOD. Simply optimizing the model on OOD test samples may lead to severe performance degradation on ID test samples. We empirically validate the existence of this issue in Figure 3, where the updated model has a consistently lower accuracy on ID test samples than the original model.

Moreover, existing entropy-based test-time adaptation methods like Tent [12] and SAR [18] consistently encourage producing one-hot predictions with high confidence. However, in practice, incoming test samples can be severely corrupted [9], inheriting irreducible data uncertainty. Considering the data uncertainty, these test samples ideally should be predicted with relatively low confidence. Nevertheless, the data uncertainty is often overlooked by methods based on entropy minimization. Consequently, the adapted model often produces highly confident predictions (*called overconfidence*), even when the test samples are uncertain. Such misleading predictions raise potential safety concerns for real-world application scenarios. We empirically demonstrate the issue of overconfidence in Figure 7(a) and Table 2.

4 UNCERTAINTY-CALIBRATED EFFICIENT ANTI-FORGETTING TEST-TIME ADAPTATION

In this section, we first propose an **Efficient Anti-forgetting Test-time Adaptation (EATA)** method, which aims to improve the efficiency of test-time adaptation (TTA) and tackle the catastrophic forgetting issue brought by existing TTA strategies simultaneously. EATA consists of two strategies. **1) Sample-efficient entropy minimization** (c.f. Section 4.1) aims to conduct efficient adaptation relying on an active sample selection strategy. Here, the sample selection process is to choose only active samples for backward propagation and therefore improve the overall TTA efficiency (*i.e.*, less gradient backward propagation). To this end, we devise an active sample selection score, denoted by $S(\mathbf{x})$, to detect those reliable and non-redundant test samples from the test set for TTA. **2) Anti-forgetting weight regularization** (c.f. Section 4.2) seeks to alleviate knowledge forgetting by enforcing that the parameters, important for the ID domain, do not change too much in TTA. In this way, the catastrophic forgetting issue can be significantly alleviated. We illustrate EATA in Figure A in Supplementary.

To further address the overconfidence issue, we propose an **Efficient Anti-forgetting Test-time Adaptation with Calibration (EATA-C)** method. As shown in Figure 1, we introduce a new consistency-based test-time learning objective for model uncertainty reduction (c.f. Section 4.3), follow up a min-max entropy regularizer to re-calibrate the prediction uncertainty according to the inherent data uncertainty (c.f. Section 4.4).

4.1 Sample Efficient Entropy Minimization

For efficient test-time adaptation, we propose an active sample identification strategy to select samples for backward propagation. Specifically, we design an active sample selection score for each sample, denoted by $S(\mathbf{x})$, based on two criteria: 1) samples should be **reliable** for test-time adaptation, and 2) the samples involved in optimization should be **non-redundant**. By setting $S(\mathbf{x})=0$ for non-active samples, namely the unreliable and redundant samples, we can reduce unnecessary backward computation during test-time adaptation, thereby improving the prediction efficiency.

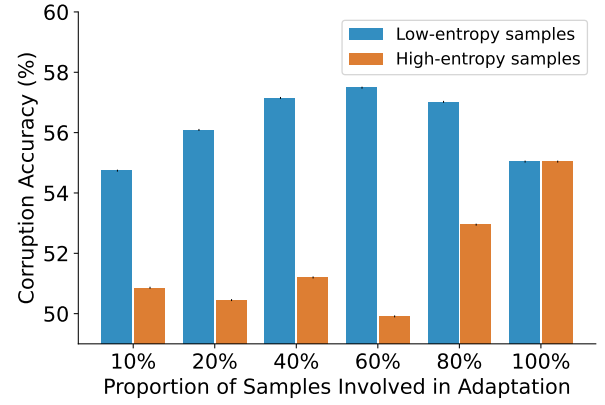


Fig. 2. Effect of different test samples in test-time entropy minimization [12]. We adapt a model on partial samples (top $p\%$ samples with the highest or lowest entropy values), and then evaluate the adapted model on all test samples. Results are obtained on ImageNet-C (Gaussian noise, level 3) and ResNet-50 (base accuracy is 27.6%). Introducing more samples with high entropy values into adaptation will hurt the adaptation performance.

Relying on the sample score $S(\mathbf{x})$, following [12], [14], we use entropy loss for model adaptations. Then, the sample-efficient entropy minimization is to minimize the following objective:

$$\min_{\Theta} S(\mathbf{x})E(\mathbf{x}; \Theta) = -S(\mathbf{x}) \sum_{y \in \mathcal{C}} f_{\Theta}(y|\mathbf{x}) \log f_{\Theta}(y|\mathbf{x}), \quad (2)$$

where \mathcal{C} is the model output space. Here, the entropy loss $E(\cdot)$ is calculated over a batch of samples each time (similar to Tent [12]) to avoid a trivial solution, *i.e.*, assigning all probability to the most probable class. For efficient adaptation, we update $\hat{\Theta} \subseteq \Theta$ with the affine parameters of all normalization layers.

Reliable Sample Identification. Our intuition is that different test samples produce various effects in adaptation. To verify this, we conduct a preliminary study, where we select different proportions of samples (the samples are pre-sorted according to their entropy values $E(\mathbf{x}; \Theta)$) for adaptation, and the resulting model is evaluated on all test samples. From Figure 2, we find that: 1) adaptation on low-entropy samples makes more contribution than high-entropy ones, and 2) adaptation on test samples with very high entropy may hurt performance. The possible reason is that predictions of high-entropy samples are uncertain, so their gradients produced by entropy loss may be biased and unreliable. Following this, we name these low-entropy samples as reliable samples. Based on the above observation, we propose an entropy-based weighting scheme to identify reliable samples and emphasize their contributions during adaptation. Formally, the entropy-based weight is given by:

$$S^{ent}(\mathbf{x}) = \frac{1}{\exp[E(\mathbf{x}; \Theta) - E_0]} \cdot \mathbb{I}_{\{E(\mathbf{x}; \Theta) < E_0\}}(\mathbf{x}), \quad (3)$$

where $\mathbb{I}_{\{\cdot\}}(\cdot)$ is an indicator function, $E(\mathbf{x}; \Theta)$ is the predicted entropy regarding sample \mathbf{x} , and E_0 is a pre-defined threshold. The above weighting function excludes high-entropy samples from adaptation and assigns higher weights to test samples with lower prediction uncertainties, allowing them to contribute more to model updates. Note that evaluating $S^{ent}(\mathbf{x})$ does not involve any gradient back-propagation.

Non-redundant Sample Identification. Although Eqn. (3) helps to exclude partial unreliable samples, the remaining test

samples may still have redundancy. For example, given two test samples that are mutually similar and both have a lower prediction entropy than E_0 , we still need to perform gradient back-propagation for each of them according to Eqn. (3). However, this is unnecessary as these two samples produce similar gradients for model adaptation.

To further improve efficiency, we propose to exploit the samples that can produce different gradients for model adaptation. Recall that the entropy loss only relies on final model outputs (*i.e.*, classification logits), we further filter samples by ensuring the remaining samples have diverse model outputs. To this end, one straightforward method is to save the model outputs of all previously seen samples, and then compute the similarity between the outputs of incoming test samples and all saved model outputs for filtering. However, this method is computationally expensive at test time and memory-consuming with the increase of test samples.

To address this, we exploit an exponential moving average technique to track the average model outputs of all seen test samples used for model adaptation. To be specific, given a set of model outputs of test samples, the moving average vector is updated recursively:

$$\mathbf{m}^t = \begin{cases} \bar{\mathbf{y}}^1, & \text{if } t = 1 \\ \alpha \bar{\mathbf{y}}^t + (1 - \alpha) \mathbf{m}^{t-1}, & \text{if } t > 1 \end{cases}, \quad (4)$$

where $\bar{\mathbf{y}}^t = \frac{1}{n} \sum_{k=1}^n \hat{\mathbf{y}}_k^t$ is the average model prediction of a mini-batch of n test samples at the iteration t , and $\alpha \in [0, 1]$. Following that, given a new test sample \mathbf{x} received at iteration $t > 1$, we compute the cosine similarity between its prediction $f_{\Theta}(\mathbf{x})$ and the moving average \mathbf{m}^{t-1} (*i.e.*, $\cos(f_{\Theta}(\mathbf{x}), \mathbf{m}^{t-1})$), which is then used to determine the diversity-based weight:

$$S^{div}(\mathbf{x}) = \mathbb{I}_{\{\cos(f_{\Theta}(\mathbf{x}), \mathbf{m}^{t-1}) < \epsilon\}}(\mathbf{x}), \quad (5)$$

where ϵ is a pre-defined threshold for cosine similarities. The overall sample-adaptive weight is then given by:

$$S(\mathbf{x}) = S^{ent}(\mathbf{x}) \cdot S^{div}(\mathbf{x}), \quad (6)$$

which combines both entropy-based (as in Eqn. 3) and diversity-based terms (as in Eqn. 5). Since we only perform gradient back-propagation for test samples with $S(\mathbf{x}) > 0$, the algorithm efficiency is further improved.

Remark. Given M test samples $\mathcal{D}_{test} = \{\mathbf{x}_j\}_{j=1}^M$, the total number of reduced backward computations is given by $\mathbb{E}_{\mathbf{x} \sim \mathcal{D}_{test}}[\mathbb{I}_{\{S(\mathbf{x})=0\}}(\mathbf{x})]$, which is jointly determined by test data \mathcal{D}_{test} , entropy threshold E_0 , and cosine similarity threshold ϵ .

4.2 Anti-Forgetting with Fisher Regularization

In this section, we propose a new weighted Fisher regularizer (called anti-forgetting regularizer) to alleviate the catastrophic forgetting issue caused by test-time adaptation, *i.e.*, the performance of a test-time adapted model may significantly degrade on in-distribution (ID) test samples. We achieve this through weight regularization, which only affects the loss function and does not incur any additional computational overhead for model adaptation. To be specific, we apply an importance-aware regularizer \mathcal{R} to prevent model parameters, important for the in-distribution domain, from changing too much during the test-time adaptation process [23]:

$$\mathcal{R}(\tilde{\Theta}, \tilde{\Theta}^o) = \sum_{\theta_i \in \tilde{\Theta}} \omega(\theta_i) (\theta_i - \theta_i^o)^2, \quad (7)$$

where $\tilde{\Theta}$ are parameters used for model update and $\tilde{\Theta}^o$ are the corresponding parameters of the original model. $\omega(\theta_i)$ denotes the importance of θ_i and we measure it via the diagonal Fisher information matrix as in elastic weight consolidation [23]. Here, the calculation of Fisher information $\omega(\theta_i)$ is non-trivial since we are inaccessible to any labeled training data. For the convenience of presentation, we leave the details of calculating $\omega(\theta_i)$ in the next subsection.

After introducing the anti-forgetting regularizer, the final optimization formula for EATA is formulated as:

$$\min_{\tilde{\Theta}} S(\mathbf{x}) E(\mathbf{x}; \Theta) + \beta \mathcal{R}(\tilde{\Theta}, \tilde{\Theta}^o), \quad (8)$$

where β is a trade-off parameter, $S(\mathbf{x})$ and $E(\mathbf{x}; \Theta)$ are defined in Eqn. (2).

Measurement of Weight Importance $\omega(\theta_i)$. The calculation of Fisher information typically involves a set of labeled ID training samples. However, in our problem setting, we are inaccessible to training data and the test samples are only unlabeled, which makes it non-trivial to measure the weight importance. To conquer this, we first collect a small set of unlabeled ID test samples $\{\mathbf{x}_q\}_{q=1}^Q$, and then use the original trained model $f_{\Theta}(\cdot)$ to predict all these samples for obtaining the corresponding hard pseudo-label \hat{y}_q . Following that, we construct a pseudo-labeled ID test set $\mathcal{D}_F = \{\mathbf{x}_q, \hat{y}_q\}_{q=1}^Q$, based on which we calculate the fisher importance of model weights by:

$$\omega(\theta_i) = \frac{1}{Q} \sum_{\mathbf{x}_q \in \mathcal{D}_F} \left(\frac{\partial}{\partial \theta_i} \mathcal{L}_{CE}(f_{\Theta}(\mathbf{x}_q), \hat{y}_q) \right)^2, \quad (9)$$

where \mathcal{L}_{CE} is the cross-entropy loss. Here, we only need to calculate $\omega(\theta_i)$ once before performing test-time adaptation. Once calculated, we keep $\omega(\theta_i)$ fixed and apply it to any types of distribution shifts. Moreover, the unlabeled ID test samples are collected based on out-of-distribution detection techniques [56], [57], which are easy to implement. Note that there is no need to collect too many ID test samples for calculating $\omega(\theta_i)$, *e.g.*, 500 samples are enough for the ImageNet-C dataset. More empirical studies regarding this can be found in Figure 5.

4.3 Consistency-Based Uncertainty Minimization

As mentioned in Section 4.1, EATA enhances model performance by minimizing prediction entropy. This strategy aims to reduce uncertainty in predictions and learn a decision boundary in the low-density regions of the test samples [58], [59]. However, a persistent challenge with entropy minimization is its tendency to yield overly certain predictions, even in cases where the test samples themselves are inherently uncertain, such as severely corrupted images [9]. Thus, EATA may still result in overconfident predictions that fail to accurately account for the inherent data uncertainty. To address this, we further propose EATA with Calibration (EATA-C), shall be depicted in Sections 4.3 and 4.4.

In EATA-C, we first propose a consistency-based loss to quantify and optimize the model uncertainty. Our method is inspired by MC Dropout [60], which has shown promising performance in estimating the model uncertainty through the divergence of multiple dropout-enabled predictions. In our context, considering adaptation efficiency, we define the model uncertainty as the KL divergence [61] between the full network prediction and randomly sampled sub-network prediction. Here, we use only two predictions and the former is indispensable since we select it as the final

Algorithm 1 The pipeline of proposed EATA and EATA-C.

Input: Test samples $\mathcal{D}_{test} = \{\mathbf{x}_j\}_{j=1}^M$, the trained model $f_{\Theta}(\cdot)$,
 ID samples $\mathcal{D}_F = \{\mathbf{x}_q\}_{q=1}^Q$, batch size B .
 1: **for** a batch $\mathcal{X} = \{\mathbf{x}_b\}_{b=1}^B$ in \mathcal{D}_{test} **do**
 2: Calculate predictions \hat{y} for all $\mathbf{x} \in \mathcal{X}$ via $f_{\Theta}(\cdot)$.
 3: **For** EATA:
 4: Calculate sample selection score $S(\mathbf{x})$ via Eqn. (6).
 5: Update model $(\tilde{\Theta} \subseteq \Theta)$ with Eqn. (8).
 6: **For** EATA-C:
 7: Select reliable and distinct samples \mathcal{X}_s via Eqn. (15).
 8: Sample $f_{\Theta_{sub}}(\cdot)$ from $f_{\Theta}(\cdot)$ via stochastic depth [63].
 9: Calculate predictions \hat{y}_{sub} for $\mathbf{x} \in \mathcal{X}_s$ via $f_{\Theta_{sub}}(\cdot)$.
 10: Compute consistency loss $\mathcal{L}_c(\mathbf{x})$ based on Eqn. (10)
 11: Calibrate confidence with entropy loss via Eqn. (12)
 12: Update model $(\tilde{\Theta} \subseteq \Theta)$ with Eqn. (14).
 13: **end for**
Output: The predictions $\{\hat{y}\}_{j=1}^M$ for all $\mathbf{x} \in \mathcal{D}_{test}$.

prediction. Thus, at test time, we minimize divergence to encourage consistent predictions instead of confidence-related entropy loss, thereby alleviating the overconfidence issue.

Consistency Loss. Formally, let $\hat{y} = f_{\Theta}(\mathbf{x})$ be the prediction of the full network w.r.t. sample \mathbf{x} , and $\hat{y}_{sub} = f_{\Theta_{sub}}(\mathbf{x})$ be that of the sub-network. The consistency loss is defined as follows:

$$\mathcal{L}_c(\mathbf{x}) = D_{KL}(\hat{y}_{sub}, \hat{y}_{fuse}), \quad (10)$$

$$\hat{y}_{fuse} = (\hat{y} + (1 - p) \cdot \hat{y}_{sub}) / (2 - p), \quad (11)$$

where $D_{KL}(\cdot || \cdot)$ denotes Kullback-Leibler divergence [61] and p is a constant for balancing. Here, we calculate the divergence between \hat{y} and \hat{y}_{fuse} (rather than \hat{y}_{sub}), since encouraging the sub-network to achieve the same performance as the full one is relatively hard. Thus, inspired by label smoothing [62], we softly fuse \hat{y} and \hat{y}_{sub} in Eqn. (11) for divergence optimization. Note that, during optimization, we conduct a unidirectional alignment from the sub-network to the full network, as the full network typically exhibits stronger generalization capabilities. To this end, we detach the gradient from \hat{y} and concentrate the optimization solely on \hat{y}_{sub} . This strategy is designed to facilitate knowledge transfer from the full network to its sub-network, thereby enhancing the sub-network’s performance while simultaneously reducing the model uncertainty of the full network.

Remark on Efficiency. Although consistency loss requires two forward passes from both the full network and the sub-network for each sample, the full network’s forward pass is gradient-free without back-propagation and the sub-network’s forward/backward pass is less computationally intensive. Moreover, we only perform sub-network’s forward/backward pass on the selected reliable and non-redundant samples as outlined in Algorithm 1. As a result, the use of consistency loss remains efficient.

4.4 Calibrated Min-Max Entropy Regularization

In this section, we re-calibrate the model’s prediction uncertainty in a manner that is sensitive to individual samples. This process involves categorizing samples into two distinct groups—‘certain’ and ‘uncertain’—based on the aforementioned prediction consistency. This identification is achieved by comparing the predicted labels between the full network and a sub-network. Samples exhibiting mismatched predictions are deemed ‘uncertain’, indicating either

high intrinsic data uncertainty or a high level of complexity that challenges the model’s recognition capability. For these uncertain samples, we aim to lower their predictive confidence. This is achieved by maximizing the prediction entropy, effectively acknowledging the model’s lack of confidence in these cases. Conversely, for samples where predictions are consistent, labeled as ‘certain’, we conduct the opposite strategy, *i.e.*, boosting prediction confidence through entropy minimization. Formally, this min-max entropy regularization optimization problem is defined by:

$$\min_{\tilde{\Theta}_{sub}} C(\mathbf{x}) E(\mathbf{x}; \Theta_{sub}), \quad (12)$$

$$C(\mathbf{x}) = \begin{cases} 1, & \text{if } \arg \max(\hat{y}) = \arg \max(\hat{y}_{sub}), \\ -1, & \text{if } \arg \max(\hat{y}) \neq \arg \max(\hat{y}_{sub}), \end{cases} \quad (13)$$

where \hat{y} and \hat{y}_{sub} denote the prediction of the full and sub-network respectively, Θ_{sub} denotes the parameters of the sub-network and $\tilde{\Theta}_{sub} \subset \Theta_{sub}$ denotes parameters involved in model adaptation. Note that we only update the affine parameters of the sub-network considering efficiency as mentioned in Section 4.3.

Overall Objective. The methods proposed in Sections 4.3 and 4.4 are devised to address the overconfident issue in TTA, but still suffer from catastrophic forgetting when the important model weights for the in-distribution domain are modified significantly during adaptation. Therefore, we jointly optimize the model with the anti-forgetting regularizer and further reduce the required backward computations with the active sample selection criterion proposed in EATA. Then, the overall objective of EATA-C can be formulated as:

$$\min_{\tilde{\Theta}} S_c(\mathbf{x}) \left(\mathcal{L}_c(\mathbf{x}) + \alpha C(\mathbf{x}) E(\mathbf{x}; \Theta_{sub}) \right) + \beta \mathcal{R}(\tilde{\Theta}, \tilde{\Theta}^o). \quad (14)$$

where α and β are balance factors, $\mathcal{R}(\tilde{\Theta}, \tilde{\Theta}^o)$ is the fisher regularizer defined in Eqn. (7), and $S_c(\mathbf{x})$ is the joint indicator function in Eqn. (3) and Eqn. (5) to select reliable and non-redundant samples. To be specific, $S_c(\mathbf{x})$ is defined by:

$$S_c(\mathbf{x}) = S^{div}(\mathbf{x}) \cdot \mathbb{I}_{\{E(\mathbf{x}; \Theta) < E_0\}}(\mathbf{x}). \quad (15)$$

We summarize the overall pipeline of our proposed EATA-C and EATA in Algorithm 1.

5 EXPERIMENTS

Datasets and Models. We conduct experiments on three benchmarks datasets for OOD generalization, *i.e.*, ImageNet-C [9] (contains corrupted images in 15 types of 4 main categories and each type has 5 severity levels) and ImageNet-R [65] for image classification, and ACDC [66] for semantic segmentation. We use ResNet-50 (R-50) [1] and ViTBase (ViT) [67] for ImageNet experiments, and Segformer-B5 [68] for ACDC [66] experiments. The models are trained on ImageNet or CityScapes [69] training set with stochastic depth regularization [63] and then tested on clean or the above OOD test sets.

Compared Methods. We compare with the following state-of-the-art methods. BN adaptation [32] updates batch normalization statistics on test samples. Tent [12] minimizes the entropy of test samples during testing. MEMO [14] maximizes the prediction consistency of different augmented copies regarding a given test sample. CoTTA [64] minimizes the cross entropy between the predictions of the student network and its mean teacher at test time. SAR [18] selects reliable samples to perform test time sharpness-aware entropy minimization. We denote EATA without weight

TABLE 2

Comparison with state-of-the-art methods on ImageNet-C with the highest severity level 5 regarding **Corruption Accuracy(%, \uparrow)** and **Expected Calibration Error(%, \downarrow)**. “BN” and “LN” denote batch and layer normalization, respectively. The **bold** number indicates the best result and the underlined number indicates the second best result. All results are evaluated under the **lifelong adaptation scenario** except for Tent [12] and MEMO [14], which suffer severely from error accumulation. We use * and \dagger to denote episodic and single-domain adaptation, respectively.

Model	Method	Metric	Noise			Blur				Weather				Digital				Average		
			Gauss.	Shot	Impul.	Defoc.	Glass	Motion	Zoom	Snow	Frost	Fog	Brit.	Contr.	Elastic	Pixel	JPEG	Avg.	#Forwards	#Backards
R-50 (BN)	Source	Acc. ECE	1.8 16.6	3.0 16.1	1.7 15.9	18.2 1.8	10.1 10.7	13.4 10.7	20.8 14.7	14.0 25.3	22.1 12.9	21.9 16.7	58.7 <u>2.3</u>	5.3 <u>6.7</u>	17.6 22.9	22.1 10.5	37.5 6.0	17.88 12.64	50,000	0
	BN Adapt	Acc. ECE	15.8 1.1	16.7 0.8	15.3 1.0	18.7 <u>3.0</u>	19.3 1.3	29.8 0.8	41.7 3.4	35.8 1.1	35.0 1.0	50.5 5.4	65.9 1.4	18.1 7.6	49.3 4.3	51.7 <u>3.8</u>	42.0 4.8	33.70 2.72	50,000	0
	Tent [†]	Acc. ECE	28.0 11.7	30.1 11.2	28.1 11.1	29.9 12.6	29.5 12.3	42.2 7.7	49.7 5.4	46.2 6.5	41.5 8.8	57.7 <u>3.4</u>	<u>67.1</u> 2.9	30.0 21.9	55.7 3.5	58.3 3.7	52.5 <u>4.0</u>	43.11 8.46	50,000	50,000
	MEMO*	Acc. ECE	6.8 24.1	8.5 24.2	7.5 22.9	20.5 5.3	13.4 19.3	19.8 14.8	25.8 23.4	22.1 30.4	27.7 18.7	27.6 24.6	60.9 7.2	11.3 14.9	24.4 29.4	32.2 19.3	37.9 13.6	23.09 19.47	50,000×65	50,000×64
	CoTTA	Acc. ECE	19.9 <u>3.6</u>	31.8 17.4	35.3 21.5	30.4 27.8	34.4 30.4	40.2 31.2	43.2 31.6	39.3 33.2	38.6 34.2	47.7 32.5	51.8 33.1	36.0 36.0	43.5 34.2	46.7 36.1	43.1 35.9	38.80 29.25	152,315	50,000
	SAR	Acc. ECE	29.6 3.7	38.4 7.4	<u>37.8</u> 9.1	31.5 14.4	32.8 15.1	41.4 12.6	48.6 9.6	42.9 11.7	40.2 13.3	53.3 8.4	63.7 7.0	37.7 16.8	53.0 8.5	56.3 8.4	52.3 8.5	43.96 10.29	85,964	68,145
	EATA (Ours)	Acc. ECE	<u>35.6</u> 10.5	<u>38.7</u> 13.4	37.5 14.7	<u>35.9</u> 18.5	<u>36.1</u> 18.5	<u>47.6</u> 14.7	53.1 12.8	<u>50.6</u> 14.1	<u>45.6</u> 16.1	<u>59.5</u> 11.6	67.1 10.4	<u>45.2</u> 18.6	57.6 13.3	<u>59.8</u> 13.1	<u>55.4</u> 13.9	<u>48.36</u> 14.28	50,000	29,721
	EATA-C (Ours)	Acc. ECE	37.2 7.1	40.9 <u>6.7</u>	39.9 <u>7.2</u>	36.6 10.1	37.1 <u>9.5</u>	48.5 <u>5.9</u>	<u>52.7</u> <u>4.9</u>	51.9 <u>4.8</u>	47.2 <u>5.8</u>	60.4 3.2	67.0 3.2	49.0 6.0	<u>57.6</u> <u>4.0</u>	60.1 3.9	56.1 3.9	49.48 <u>5.74</u>	83,312	33,312
ViT (LN)	Source	Acc. ECE	12.9 14.2	17.6 11.3	11.7 15.2	34.4 2.2	27.7 <u>8.2</u>	43.7 <u>6.0</u>	36.2 <u>10.7</u>	43.4 <u>7.5</u>	45.4 8.3	52.8 5.0	73.3 2.1	45.5 2.3	37.9 12.2	54.7 4.1	60.2 6.0	39.84 <u>7.48</u>	50,000	0
	Tent [†]	Acc. ECE	33.4 24.1	42.1 10.1	41.4 11.7	48.8 8.6	45.2 10.4	54.9 7.5	48.2 12.4	55.6 8.0	55.1 <u>8.0</u>	64.4 <u>4.8</u>	75.2 <u>2.4</u>	62.5 <u>5.2</u>	51.6 <u>10.0</u>	65.5 4.3	65.0 4.1	53.92 8.78	50,000	50,000
	MEMO*	Acc. ECE	32.2 33.0	35.1 32.5	32.6 33.2	37.5 36.7	28.5 45.7	43.3 41.0	40.1 47.2	45.2 39.8	47.0 38.8	53.9 33.7	73.3 20.0	53.3 26.7	39.6 48.5	59.5 30.4	62.8 27.2	45.60 35.63	50,000×65	50,000×64
	CoTTA	Acc. ECE	45.6 9.0	<u>58.8</u> 15.8	<u>58.4</u> 21.0	40.1 29.3	50.9 28.3	50.4 29.1	44.4 34.5	46.1 29.8	51.4 29.6	52.2 30.0	57.7 29.2	36.5 36.3	53.9 29.0	55.8 31.2	55.4 31.8	50.51 27.59	50,000×3	50,000
	SAR	Acc. ECE	43.1 8.0	50.8 8.4	52.9 9.5	50.4 9.1	51.0 11.4	57.5 9.6	53.2 13.0	58.6 9.9	61.2 9.6	66.0 7.8	76.1 4.5	61.2 10.0	54.7 13.8	67.8 7.5	67.7 7.5	58.15 9.30	91,605	82,277
	EATA (Ours)	Acc. ECE	<u>50.5</u> 10.6	55.6 13.9	56.0 15.7	<u>54.9</u> 16.4	<u>56.3</u> 17.3	<u>61.1</u> 15.9	<u>59.8</u> 17.5	<u>64.3</u> 14.8	<u>64.0</u> 15.7	<u>70.1</u> 12.8	<u>77.4</u> 9.0	<u>65.5</u> 15.4	<u>63.1</u> 17.5	<u>70.4</u> 13.3	<u>69.5</u> 13.9	<u>62.57</u> 14.63	50,000	36,688
	EATA-C (Ours)	Acc. ECE	56.8 5.2	60.2 5.1	59.8 5.9	58.0 <u>7.1</u>	60.9 6.2	65.2 5.6	65.5 5.9	69.7 5.0	67.8 5.0	74.0 4.1	78.9 3.3	66.7 5.4	70.3 4.7	74.1 <u>4.2</u>	71.8 <u>4.7</u>	66.65 5.14	83,184	33,184

TABLE 3

Comparison on ImageNet-R. Results are evaluated in the single-domain adaptation scenario. We use * to denote episodic adaptation.

Model	Acc. (%)	ECE (%)	#Forwards	#Backwards
ResNet-50(BN)	38.0	17.7	30,000	0
• BN [32]	40.4(+2.4)	13.4(−4.3)	30,000	0
• Tent [12]	42.3(+4.3)	17.8(+0.1)	30,000	30,000
• MEMO* [14]	41.9(+3.9)	26.9(+9.2)	30,000 \times 65	30,000 \times 64
• CoTTA [64]	42.4(+4.4)	15.8(−1.9)	90,000	30,000
• SAR [18]	42.7(+4.7)	14.6(−3.1)	47,755	32,877
• EATA (Ours)	44.9(+6.9)	16.7(−1.0)	30,000	5,417
• EATA-C (Ours)	47.1 (+9.1)	13.3 (−4.4)	35,122	5,122
ViT(LN)	52.5	5.0	30,000	0
• Tent [12]	54.2(+1.7)	7.4(+2.4)	30,000	30,000
• MEMO* [14]	57.5(+5.0)	32.1(+27.1)	30,000 \times 65	30,000 \times 64
• CoTTA [64]	56.4(+3.9)	7.4(+2.4)	90,000	30,000
• SAR [18]	55.0(+2.5)	5.2(+0.2)	47,119	33,844
• EATA (Ours)	58.2(+5.7)	5.8(+0.8)	30,000	6,053
• EATA-C (Ours)	64.2 (+11.7)	3.9 (−1.1)	36,395	6,395

regularization in Eqn. (7) as **efficient test-time adaptation (ETA)**. More ablative methods can be found in Table 6.

Adaptation Scenarios. We conduct experiments under three adaptation scenarios: 1) *Episodic*, the model parameters will be reset immediately after each optimization step of a test sample or batch; 2) *Single-domain*, the model is online adapted through the entire evaluation of one given test dataset (e.g., gaussian noise level 5 of ImageNet-C). Once the adaptation on this dataset is finished, the model parameters will be reset; 3) *Lifelong*, the model is online adapted and the parameters will never be reset (as shown in Figure 3 (Right)), which is more challenging but practical.

Evaluation Metrics. 1) Clean accuracy/error (%) on original in-

distribution (ID) test samples, e.g., the original test images of ImageNet. Note that we measure the clean accuracy of all methods via (re)adaptation; 2) Out-of-distribution (OOD) accuracy/error (%) on OOD test samples, e.g., the corruption accuracy on ImageNet-C; 3) Expected Calibration Error (ECE) [70] on OOD test samples, which measures the average discrepancies between model’s confidence and accuracy within multiple confidence intervals; 4) The number of forward and backward passes during the entire TTA process. Note that the fewer #forwards and #backwards indicate less computation, leading to higher efficiency.

Implementation Details. For test time adaptation, we use SGD as the update rule, with a momentum of 0.9 and a batch size of 64. In EATA and ETA, the learning rate is set to 0.00025/0.001 for ResNet-50/ViTBase on ImageNet, and 7.5×10^{-5} on ACDC, respectively (following Tent, SAR and CoTTA). In EATA-C, the learning rate is set to 0.005/0.1 for ResNet-50/ViTBase on ImageNet, and 0.0005 on ACDC, respectively. The sub-network is obtained via stochastic depth regularization [63] with a drop ratio of 0.2/0.6 for ImageNet/ACDC. For both EATA and EATA-C, we use 2,000/20 samples for ImageNet/ACDC to calculate $\omega(\theta_i)$ in Eqn. (9). More details are put in Supplementary.

5.1 Comparisons w.r.t. OOD Performance, Efficiency and Calibration Error

Results on ImageNet-C. From the results, our EATA and EATA-C significantly outperform the considered methods over both ResNet-50 and ViTBase regarding the classification accuracy, suggesting our effectiveness. With our sample-adaptive entropy loss, EATA achieves a large performance gain over the counterpart Tent (e.g., 33.4% \rightarrow 50.5% on Gaussian noise with ViTBase), verifying that

TABLE 4

Semantic segmentation results (mIoU in %) on the Cityscapes-to-ACDC lifelong test-time adaptation scenario. The model is continually adapted to the four adverse conditions for ten rounds without model reset. All results are evaluated based on the Segformer-B5 architecture. Following [64], we only show the results of the first, fourth, seventh, and last rounds due to page limits. Full results can be found in the supplementary material.

Round	1				4				7				10				All
Condition	Fog	Night	Rain	Snow	Fog	Night	Rain	Snow	Fog	Night	Rain	Snow	Fog	Night	Rain	Snow	Mean
Source	69.1	40.3	59.7	57.8	69.1	40.3	59.7	57.8	69.1	40.3	59.7	57.8	69.1	40.3	59.7	57.8	56.7
BN Stats Adapt	62.3	38.0	54.6	53.0	62.3	38.0	54.6	53.0	62.3	38.0	54.6	53.0	62.3	38.0	54.6	53.0	52.0 _(-4.7)
Tent (lifelong)	69.0	40.2	60.0	57.3	66.6	36.6	58.9	54.2	64.6	33.4	55.9	51.6	62.5	30.4	52.6	48.7	52.7 _(-4.0)
CoTTA	70.9	41.1	62.4	59.7	70.8	40.6	62.6	59.7	70.8	40.5	62.6	59.7	70.8	40.5	62.6	59.7	58.4 _(+1.7)
EATA	69.1	40.5	59.8	58.1	69.3	41.8	60.1	58.6	68.8	42.5	59.4	57.9	67.9	42.8	57.7	56.3	57.0 _(+0.3)
EATA-C	71.0	44.3	63.1	61.1	72.0	47.3	64.9	63.8	71.8	48.2	64.2	64.2	72.0	48.7	64.3	64.1	61.6 _(+4.9)

removing samples with unreliable gradients and tackling samples differently benefits the test-time adaptation. More critically, EATA-C outperforms CoTTA and SAR consistently in all 15 corruption types (while EATA fails to achieve this), demonstrating the effectiveness to reduce model uncertainty with our consistency loss. Note that besides achieving strong OOD performance, EATA also alleviates the forgetting on ID samples (see Figure 3), showing the effectiveness of our anti-forgetting regularization without limiting the learning ability during adaptation (see also Table 6 for ablation).

As for efficiency, the required average backward number of our EATA is 29,721 on ResNet-50, which is much fewer than the method that needs multiple data augmentations (*i.e.*, MEMO is $50,000 \times 64$) or that requires multiple rounds of optimizations (*e.g.*, SAR is 68,145 on ResNet-50). Compared with Tent, EATA reduces the average #backward (*e.g.*, $50,000 \rightarrow 29,721$ on ResNet-50) by excluding samples with high prediction entropy and samples that are similar out of test-time optimization. In this sense, our method only needs to adapt for partial samples, resulting in higher efficiency. While EATA-C requires more forward passes, its forward passes on all test samples using the full network are gradient-free, and the more lightweight sub-network’s forward/backward passes are conducted only on the selected reliable and non-redundant samples, maintaining comparable efficiency. Note that although optimization-free methods (such as BN adaptation) do not need backward updates, their OOD performances are limited.

In terms of calibration, existing methods consistently exhibit severe overconfidence (*e.g.*, MEMO and CoTTA are 35.63% and 27.59% on ECE with ViTBase), suggesting that overconfidence is a prevalent issue in the unsupervised test-time adaptation. Note that by filtering unreliable samples to mitigate error accumulation, EATA achieves better calibration compared with Tent (*e.g.*, $11.7\% \rightarrow 10.5\%$ on Gaussian noise with ResNet-50). However, the miscalibration is yet significant. By further differentiating the reducible model uncertainty and the inherent data uncertainty in adaptation, our EATA-C is able to reduce the calibration error by relatively 59.8% on ResNet-50 and 64.9% on ViTBase compared with EATA, demonstrating the promising calibration effect of EATA-C on different datasets and various architectures. It is worth mentioning that while EATA-C enhances performance and efficiency, EATA-C further achieves consistent and substantial improvement over accuracy, efficiency, and calibration error compared with state-of-the-art methods, suggesting our superiority.

Results on ImageNet-R. From Table 3, our EATA consistently achieves better performance than compared methods on both ResNet-50 and ViTBase, while significantly reducing the required backward propagation (*e.g.*, **30,000** \rightarrow **5,417** on ResNet-50 over

Tent), demonstrating the effectiveness of adapting on partial samples during testing. Our EATA-C further improves performance by a large margin (+6.0% over EATA on ViTBase), while achieving the best calibration. More critically, EATA-C is the only method that reduces calibration error on both ResNet-50 and ViTBase, suggesting the superiority in managing model uncertainty and data uncertainty differently for calibrated test-time adaptation.

Results on CityScapes-to-ACDC. Following [64], we evaluate our method on semantic segmentation task in the lifelong adaptation scenario. From Table 4, EATA achieves comparative performance by filtering unreliable predictions and constraining the important weights from drastic change, while its counterpart, Tent, severely suffers from error accumulation. Moreover, by differentiating model uncertainty and data uncertainty in test-time adaptation, EATA-C achieves state-of-the-art performance, outperforming EATA by 4.6% and CoTTA by 3.2% in mIoU. More importantly, EATA-C can progressively accumulate knowledge over adaptation to improve its performance. In the first and tenth rounds of adaptation, EATA-C achieves 59.8% *vs.* 62.3% in average mIoU on the four adverse datasets, further verifying the effectiveness of our method.

5.2 Demonstration of Preventing Forgetting

In this section, we investigate the ability of our EATA in preventing ID forgetting during test-time adaptation. The experiments are conducted on ImageNet-C with ResNet-50. We measure the anti-forgetting ability by comparing the model’s clean accuracy (*i.e.*, on original validation data of ImageNet) before and after adaptation. To this end, we first perform test-time adaptation on a given OOD test set, and then evaluate the clean accuracy of the updated model. Here, we consider two adaptation scenarios: the single-domain adaptation, and the lifelong adaptation. We report the results of severity level 5 in Figure 3 and put the results of severity levels 1-4 into Supplementary.

From Figure 3, our EATA consistently outperforms Tent regarding the OOD corruption accuracy and meanwhile maintains the clean accuracy on ID data (in both two adaptation scenarios), demonstrating our effectiveness. It is worth noting that the performance degradation in lifelong adaptation scenario is much more severe (see Figure 3 **Right**). More critically, in lifelong adaptation, both the clean and corruption accuracy of Tent decreases rapidly (until degrades to 0%) after adaptation of the first three corruption types, showing that Tent in lifelong adaptation is not stable enough. In contrast, during the whole lifelong adaptation process, our EATA achieves good corruption accuracy and the clean accuracy is also very close to the clean accuracy of the model without any OOD adaptation (*i.e.*, original clean accuracy, tested using Tent). These

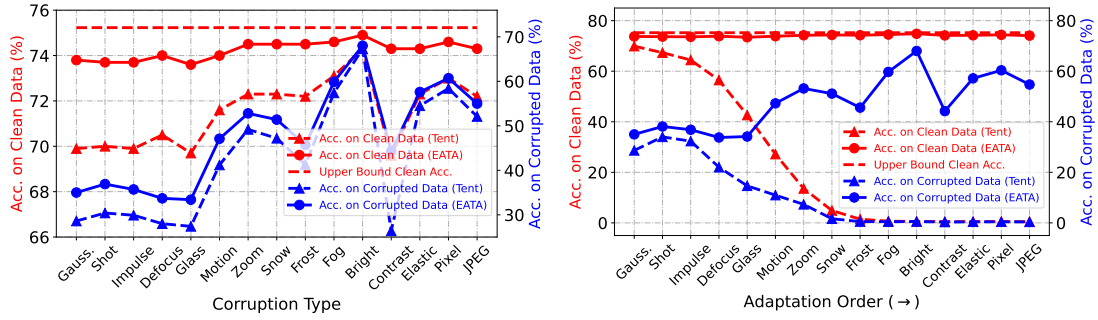


Fig. 3. Comparison of preventing forgetting on ImageNet-C (severity level 5) with ResNet-50. We record the OOD corruption accuracy on each corrupted test set and the ID clean accuracy (after OOD adaptation). In **Left**, the model parameters of both Tent and our EATA are reset before adapting to a new corruption type. In **Right**, the model performs lifelong adaptation and the parameters will never be reset, namely Tent (lifelong) and our EATA (lifelong). The upper bound clean accuracy is estimated with the source model without adaptation on corrupted OOD data, which does not suffer from forgetting. EATA achieves higher OOD accuracy and meanwhile maintains the ID clean accuracy.

results demonstrate the superiority of our anti-forgetting Fisher regularizer in terms of overcoming the forgetting on ID data.

5.3 Ablation Studies

Effect of Components in $S(\mathbf{x})$ (Eqn. 6). Our EATA accelerates test-time adaptation by excluding two types of samples out of optimization: 1) samples with high prediction entropy values (Eqn. 3) and 2) samples that are similar (Eqn. 6). We ablate both of them in Table 5. Compared with the baseline $S(\mathbf{x})=1$ (the same as Tent), introducing $S^{ent}(\mathbf{x})$ in Eqn. (3) achieves better accuracy and fewer backwards (e.g., 49.6% (37,636) vs. 33.4% (50,000) on level 5). This verifies our motivation in Figure 2 that some high-entropy samples may hurt the performance since their gradients are unreliable. When further removing some redundant samples that are similar (Eqn. 6), our EATA further reduces the number of back-propagation (e.g., 37,636 \rightarrow 28,168 on level 5) and achieves comparable OOD error (e.g., 50.4% vs. 49.6%), demonstrating the effectiveness of our sample-efficient optimization strategy.

Effect of Components in EATA-C. By further differentiating between model uncertainty and data uncertainty based on EATA, our EATA-C achieves a substantial improvement in performance, efficiency and calibration. We conduct ablation to verify their effectiveness in Table 6. Note that adapting with simply the consistency loss in Eqn. (10) already leads to a strong baseline. By re-calibrating confidence on different samples via Eqn. (12), we further mitigate the calibration error, e.g., 3.3% (Exp1) \rightarrow 2.5% (Exp3) on ECE. Compared with Exp3, Exp6 maintains comparable calibration while improving accuracy (i.e., 65.9% \rightarrow 66.4%), demonstrating that our anti-forgetting regularizer does not limit OOD adaptation. When further introducing the sample selection in Eqn. (15), EATA-C is able to effectively reduce both forward passes (i.e., 50,000 \times 2 \rightarrow 82,364) and backward passes (50,000 \rightarrow 32,364) by a large margin. Note that although accuracy and calibration are slightly compromised in EATA-C, due to the robustness of our consistency loss on corrupted images compared with Tent (see Figure 7), its improvement over the source model (65.9% vs. 39.8% on accuracy, and 3.3% vs. 7.5% on ECE) is still significant.

Entropy Constant E_0 in Eqn. (3). We evaluate our EATA with different E_0 , selected from $\{0.20, 0.25, 0.30, 0.35, 0.40, 0.45, 0.50, 0.55\} \times \ln 10^3$, where 10^3 is the class number of ImageNet. From Figure 4, our EATA achieves excellent performance when E_0 belongs to $[0.4, 0.5]$. Either a smaller or larger E_0 would hamper the performance. The reasons are mainly as follows. When E_0 is small, EATA removes too many samples during adaptation and thus

TABLE 5
Effectiveness of components in sample-adaptive weight $S(\mathbf{x})$ in EATA on ImageNet-C (Gaussian noise) with ResNet-50.

Method	Level 3		Level 5	
	Acc. (%)	#Backwards	Acc. (%)	#Backwards
Baseline ($S(\mathbf{x})=1$)	68.8	50,000	33.4	50,000
+ $S^{ent}(\mathbf{x})$ (Eqn. 3)	70.7	45,302	49.6	37,636
+ $S(\mathbf{x})$ (Eqn. 6)	70.8	36,057	50.4	28,168

TABLE 6
Effects of components in EATA-C. Results obtained on 15 corruptions of ImageNet-C (severity level 5) with ViTBase in single-domain adaptation scenario, i.e., **the model parameters are reset before adapting to a new corruption**. CL denotes consistency loss. ER denotes min-max entropy regularization. FR denotes anti-forgetting Fisher regularization. SS denotes active sample selection.

Experiment	CL	ER	FR	SS	Acc.	ECE	Average #Forwards	#Backwards
1	✓				65.6	3.3	50,000 \times 2	50,000
2		✓			53.4	4.1	50,000 \times 2	50,000
3	✓	✓			65.9	2.5	50,000 \times 2	50,000
4	✓		✓		66.0	3.3	50,000 \times 2	50,000
5		✓	✓		53.0	4.5	50,000 \times 2	50,000
6	✓	✓	✓		66.4	2.6	50,000 \times 2	50,000
7	✓			✓	65.6	4.4	83,182	33,182
8		✓		✓	52.9	3.4	73,323	23,323
9 (EATA-C)	✓	✓		✓	65.3	3.4	82,015	32,015
10	✓		✓	✓	66.2	4.3	83,429	33,429
11		✓	✓	✓	53.2	3.4	73,723	23,723
12 (EATA-C)	✓	✓	✓	✓	65.9	3.3	82,364	32,364

is unable to learn enough knowledge from the remaining samples. When E_0 is too large, some high-entropy samples would take part but contribute unreliable and harmful gradients, resulting in performance degradation. As larger E_0 leads to more backward passes, we set E_0 to $0.4 \times \ln 10^3$ for efficiency-performance trade-off and fix the proportion of 0.4 for all other ImageNet experiments. **Number of Samples for Calculating Fisher in Eqn. (9).** As described in Section 4.2, the calculation of Fisher information involves a small set of unlabeled ID samples, which can be collected via existing OOD detection techniques [57]. Here, we investigate the effect of #samples Q , selected from $\{200, 300, 500, 700, 1000, 1500, 2000, 3000\}$. From Figure 5, our EATA achieves stable performance with $Q \geq 300$, i.e., compared with ETA, the OOD performance is comparable and the clean accuracy is much higher. These results show that our EATA does not need to collect too many ID samples, which are easy to obtain in practice.

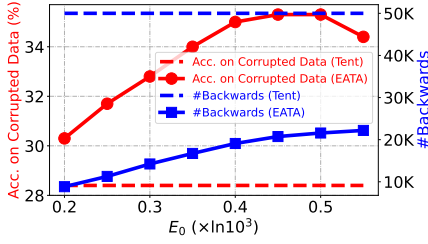


Fig. 4. Effect of different entropy margins E_0 in Eqn. (3). Results obtained on ImageNet-C(Gaussian, level 5) with ResNet-50.

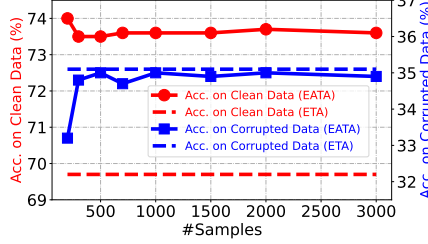


Fig. 5. Effect of #samples for calculating Fisher in Eqn. (9). Results obtained on ImageNet-C(Gaussian, level 5) with ResNet-50.

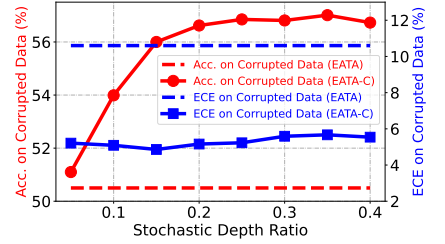


Fig. 6. Effect of different stochastic depth ratios in EATA-C. Results obtained on ImageNet-C(Gaussian, level 5) with ViTBase.

Stochastic Depth Ratio for Obtaining Sub-Network. In Eqn. (10), We generate an extra prediction from the sub-network to measure model uncertainty, where the sub-network is obtained via stochastic depth [63] throughout the experiments. We evaluate the effect of stochastic depth ratio selected from $\{0.05, 0.1, 0.15, 0.2, 0.25, 0.3, 0.35, 0.4\}$. As shown in Figure 6, our EATA-C achieves a satisfying performance-calibration trade-off when the ratio belongs to $[0.15, 0.25]$, where the full network consistently outperforms the sub-network while the sub-network retains sufficient capacity for learning. We fix the ratio to 0.2 for all other ImageNet experiments.

5.4 More Discussions

Results on Single Sample Adaptation (Batch Size $B = 1$). In our proposed methods, we conduct test-time learning over a batch of test samples each time. When batch size B equals 1, directly applying Tent and our ETA on models with batch normalization layers may fail (see Table 7), but it is not a very significant issue in practice. Actually, one can address this by either maintaining a sliding window $\{\mathbf{x}_i\}_{i=t-L}^t$ including L previous samples and the current test sample \mathbf{x}_t , or data augmentation techniques adopted in existing single sample TTA methods ([14], [33]). The first way is simple to implement and incurs only minor extra costs. From Table 7, our ETA with sliding window (ETA-wnd) works well and consistently outperforms the Tent counterpart.

Wall-clock Time Speed-up of EATA and EATA-C. In the current PyTorch version, gradient computation is conducted on the full mini-batch, even if instance-wise masks are applied. To benefit from active sample selection, in EATA, we perform one forward-only pass with B samples, and one extra forward and backward pass with B' selected samples. We achieve wall-time speed-up when setting E_0 in Eqn. (3) to $0.1 \times \ln C$, where C is the number of task classes. For ViTBase on ImageNet-C (Gaussian noise, level=5) with one Titan Xp GPU, the actual run time is 518s for Tent (33.3% accuracy), 346s for EATA (39.5% accuracy), and 402s for EATA-C (51.3% accuracy). It's also worth mentioning that in EATA-C, the sub-network's computation is not accelerated even if we select partial samples for each layer due to a similar setback. Actually, this is a more engineering problem, and an ideal implementation should further speed up both EATA and EATA-C.

Additional Memory by Fisher Regularizer. Since we only regularize the affine parameters of normalization layers, EATA needs very little extra memory. For ResNet-50 on ImageNet-C, the extra GPU memory at run time is only 9.8 MB, which is much less than that of Tent with batch size 64 (5,675 MB).

Performance under Mixed-and-Shifted Distributions. We evaluate Tent and our EATA/EATA-C on mixed ImageNet-C (level=3 or 5) that consists of 15 different corruption types/distribution shifts

TABLE 7
Effectiveness of ETA under sliding window strategy (with different window length L) for single sample adaptation with ResNet-50. We report corruption accuracy (%) on ImageNet-C (Gaussian noise, level 5).

Base ResNet-50	Tent	ETA	Tent-wnd ($L=32$)	ETA-wnd ($L=32$)	Tent-wnd ($L=64$)	ETA-wnd ($L=64$)
2.2	0.1	0.1	28.1	30.8	29.5	32.4

TABLE 8
Comparison with Tent [12] w.r.t. corruption accuracy (%) with mixture of 15 corruption types on ImageNet-C with ViTBase.

Severity	Source	Tent	EATA (ours)	EATA-C (ours)
Level=3	63.0	69.8(+6.8)	71.1(+8.1)	72.4(+9.4)
Level=5	39.8	47.0(+7.2)	58.2(+18.4)	60.4(+20.6)

(totaling 750k images). Results in Table 8 show the stability of EATA and EATA-C in large-scale and complex TTA scenarios.

Advantage of Consistency Loss over Tent [12]. We conduct a comprehensive comparison of the performance, calibration and stability between the use of consistency loss, as defined in Eqn. (10), and entropy minimization loss (*i.e.*, Tent [12]) to reduce uncertainty at test time. The experiments are conducted on ImageNet-C (Gaussian noise, level 5) with ViTBase.

In Figure 7(a), we partition the dataset into 80% and 20% for adaptation and evaluation, respectively, to show how adaptation impacts performance and calibration over time. Analyzing Figure 7(a), we discern several key findings: 1) consistency loss consistently demonstrates superior performance and calibration throughout adaptation. 2) consistency loss is more *sample-efficient*, where adapting with as few as 75 batches can significantly outperform Tent [12] that adapts with 300 batches. 3) Tent [12] shows rapid degradation in performance and calibration after convergence, which indicates that it tends to over-fit. In contrast, consistency loss maintains stable performance and calibration after convergence and continuously exhibits strong generalization throughout adaptation.

In Figures 7(b) and 7(c), we study the stability of consistency loss and Tent [12] across various combinations of learning rates and adaptation steps following [71]. As illustrated in Figure 7(b), consistency loss demonstrates remarkable performance stability and benefits from the increment of adaptation steps (*e.g.*, 55.8% \rightarrow 58.6%, the best performance under 1 and 5 adaptation steps, respectively). In contrast, Tent [12] is sensitive to the combination of learning rate and adaptation steps, where its performance may deteriorate to as low as 1%. Such a phenomenon further highlights Tent [12]'s

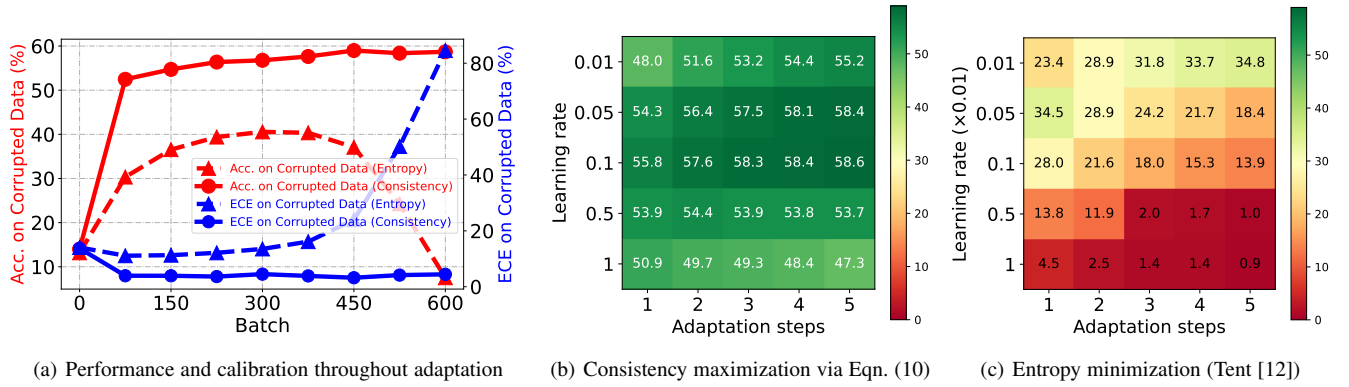


Fig. 7. Comparisons of performance, calibration and stability using consistency loss in Eqn. (10) or entropy minimization loss (i.e., Tent) on ImageNet-C (Gaussian noise, severity level=5) with ViTBase. In **Left**, we split the dataset into 80% and 20% slices to conduct adaptation and to evaluate the adapted model. We report the performance and the calibration of the adapted model every 75 batches. In the **Middle** and **Right**, we evaluate the stability of using consistency loss and Tent under various combinations of learning rates and adaptation steps per batch. Consistency loss achieves substantially higher OOD performance and better stability while maintaining lower ECE.

tendency to over-fit. In this sense, consistency loss emerges as the superior choice considering performance, calibration, stability and sample efficiency.

6 CONCLUSION

In this paper, we have proposed an Efficient Anti-forgetting Test-time Adaptation method (EATA), to improve the performance of pre-trained models on a potentially shifted test domain. To be specific, we devise a sample-efficient entropy minimization strategy that selectively performs test-time optimization with reliable and non-redundant samples. This improves the adaptation efficiency and meanwhile boosts the out-of-distribution performance. In addition, we introduce a Fisher-based anti-forgetting regularizer into test-time adaptation. With this loss, a model can be adapted continually without performance degradation on in-distribution test samples. Moreover, we design EATA with Calibration (EATA-C) for test-time adapted model’s confidence calibration. To this end, we present a consistency loss for calibrated model uncertainty reduction and a sample-aware min-max entropy regularization for confidence re-calibration, which improves the performance and calibration of test-time adaptation. Extensive experimental results on image classification and semantic segmentation demonstrate the effectiveness of our proposed methods.

REFERENCES

- [1] K. He, X. Zhang, S. Ren, and J. Sun, “Deep residual learning for image recognition,” in *IEEE Conference on Computer Vision and Pattern Recognition*, 2016, pp. 770–778.
- [2] X. Wang, R. Girshick, A. Gupta, and K. He, “Non-local neural networks,” in *IEEE Conference on Computer Vision and Pattern Recognition*, 2018, pp. 7794–7803.
- [3] R. Zeng, H. Xu, W. Huang, P. Chen, M. Tan, and C. Gan, “Dense regression network for video grounding,” in *IEEE Conference on Computer Vision and Pattern Recognition*, 2020.
- [4] R. Zeng, W. Huang, M. Tan, Y. Rong, P. Zhao, J. Huang, and C. Gan, “Graph convolutional module for temporal action localization in videos,” *IEEE Transactions on Pattern Analysis and Machine Intelligence*, 2021.
- [5] P. Chen, D. Huang, D. He, X. Long, R. Zeng, S. Wen, M. Tan, and C. Gan, “Rspnet: Relative speed perception for unsupervised video representation learning,” in *AAAI Conference on Artificial Intelligence*, vol. 1, 2021.
- [6] Y. Choi, M. Choi, M. Kim, J.-W. Ha, S. Kim, and J. Choo, “Stargan: Unified generative adversarial networks for multi-domain image-to-image translation,” in *IEEE Conference on Computer Vision and Pattern Recognition*, 2018, pp. 8789–8797.
- [7] D.-P. Fan, T. Zhou, G.-P. Ji, Y. Zhou, G. Chen, H. Fu, J. Shen, and L. Shao, “Inf-net: Automatic covid-19 lung infection segmentation from ct images,” *IEEE Transactions on Medical Imaging*, vol. 39, no. 8, pp. 2626–2637, 2020.
- [8] G. Xu, S. Niu, M. Tan, Y. Luo, Q. Du, and Q. Wu, “Towards accurate text-based image captioning with content diversity exploration,” in *IEEE Conference on Computer Vision and Pattern Recognition*, 2021, pp. 12 637–12 646.
- [9] D. Hendrycks and T. Dietterich, “Benchmarking neural network robustness to common corruptions and perturbations,” in *International Conference on Learning Representations*, 2019.
- [10] P. W. Koh, S. Sagawa, H. Marklund, S. M. Xie, M. Zhang, A. Balsubramani, W. Hu, M. Yasunaga, R. L. Phillips, I. Gao *et al.*, “Wilds: A benchmark of in-the-wild distribution shifts,” in *International Conference on Machine Learning*, 2021, pp. 5637–5664.
- [11] Y. Sun, X. Wang, Z. Liu, J. Miller, A. Efros, and M. Hardt, “Test-time training with self-supervision for generalization under distribution shifts,” in *International Conference on Machine Learning*, 2020, pp. 9229–9248.
- [12] D. Wang, E. Shelhamer, S. Liu, B. Olshausen, and T. Darrell, “Tent: Fully test-time adaptation by entropy minimization,” in *International Conference on Learning Representations*, 2021.
- [13] Y. Liu, P. Kothari, B. van Delft, B. Bellot-Gurlet, T. Mordan, and A. Alahi, “Ttt++: When does self-supervised test-time training fail or thrive?” in *Advances in Neural Information Processing Systems*, vol. 34, 2021.
- [14] M. M. Zhang, S. Levine, and C. Finn, “Memo: Test time robustness via adaptation and augmentation,” in *NeurIPS 2021 Workshop on Distribution Shifts: Connecting Methods and Applications*, 2021.
- [15] Y. Zhang, B. Hooi, L. Hong, and J. Feng, “Self-supervised aggregation of diverse experts for test-agnostic long-tailed recognition,” in *Advances in Neural Information Processing Systems*, 2022.
- [16] Q. Wang, O. Fink, L. Van Gool, and D. Dai, “Continual test-time domain adaptation,” in *IEEE Conference on Computer Vision and Pattern Recognition*, 2022.
- [17] S. Gidaris, P. Singh, and N. Komodakis, “Unsupervised representation learning by predicting image rotations,” in *International Conference on Learning Representations*, 2018.
- [18] S. Niu, J. Wu, Y. Zhang, Z. Wen, Y. Chen, P. Zhao, and M. Tan, “Towards stable test-time adaptation in dynamic wild world,” in *International Conference on Learning Representations*, 2023.
- [19] Y. Grandvalet and Y. Bengio, “Semi-supervised learning by entropy minimization,” *Advances in neural information processing systems*, vol. 17, 2004.
- [20] J. Wu, H. Fan, X. Zhang, S. Lin, and Z. Li, “Semi-supervised semantic segmentation via entropy minimization,” in *2021 IEEE International Conference on Multimedia and Expo (ICME)*. IEEE, 2021, pp. 1–6.
- [21] M. Bojarski, D. Del Testa, D. Dworakowski, B. Firner, B. Flepp, P. Goyal, L. D. Jackel, M. Monfort, U. Muller, J. Zhang *et al.*, “End to end learning for self-driving cars,” *arXiv preprint arXiv:1604.07316*, 2016.
- [22] S. M. Anwar, M. Majid, A. Qayyum, M. Awais, M. Alnowami, and M. K. Khan, “Medical image analysis using convolutional neural networks: a review,” *Journal of medical systems*, vol. 42, no. 11, pp. 1–13, 2018.
- [23] J. Kirkpatrick, R. Pascanu, N. Rabinowitz, J. Veness, G. Desjardins, A. A. Rusu, K. Milan, J. Quan, T. Ramalho, A. Grabska-Barwinska *et al.*,

- “Overcoming catastrophic forgetting in neural networks,” *Proceedings of the national academy of sciences*, vol. 114, no. 13, pp. 3521–3526, 2017.
- [24] Z. Deng, Z. Chen, S. Niu, T. Li, B. Zhuang, and M. Tan, “Efficient test-time adaptation for super-resolution with second-order degradation and reconstruction,” in *Advances in Neural Information Processing Systems*, 2024.
- [25] Z. Wen, S. Niu, G. Li, Q. Wu, M. Tan, and Q. Wu, “Test-time model adaptation for visual question answering with debiased self-supervisions,” *IEEE Transactions on Multimedia*, 2023.
- [26] O. Veksler, “Test time adaptation with regularized loss for weakly supervised salient object detection,” in *IEEE Conference on Computer Vision and Pattern Recognition*, 2023, pp. 7360–7369.
- [27] F. Azimi, S. Palacio, F. Raue, J. Hees, L. Bertinetto, and A. Dengel, “Self-supervised test-time adaptation on video data,” in *Proceedings of the IEEE/CVF Winter Conference on Applications of Computer Vision*, 2022, pp. 3439–3448.
- [28] R. Zeng, Q. Deng, H. Xu, S. Niu, and J. Chen, “Exploring motion cues for video test-time adaptation,” in *Proceedings of the 31st ACM International Conference on Multimedia*, 2023, pp. 1840–1850.
- [29] Y. Gandelsman, Y. Sun, X. Chen, and A. Efros, “Test-time training with masked autoencoders,” *Advances in Neural Information Processing Systems*, vol. 35, pp. 29 374–29 385, 2022.
- [30] A. Bartler, A. Bühler, F. Wiewel, M. Döbler, and B. Yang, “Mt3: Meta test-time training for self-supervised test-time adaption,” in *International Conference on Artificial Intelligence and Statistics*. PMLR, 2022, pp. 3080–3090.
- [31] Z. Nado, S. Padhy, D. Sculley, A. D’Amour, B. Lakshminarayanan, and J. Snoek, “Evaluating prediction-time batch normalization for robustness under covariate shift,” *arXiv preprint arXiv:2006.10963*, 2020.
- [32] S. Schneider, E. Rusak, L. Eck, O. Bringmann, W. Brendel, and M. Bethge, “Improving robustness against common corruptions by covariate shift adaptation,” in *Advances in Neural Information Processing Systems*, vol. 33, 2020, pp. 11 539–11 551.
- [33] A. Khurana, S. Paul, P. Rai, S. Biswas, and G. Aggarwal, “Sita: Single image test-time adaptation,” *arXiv preprint arXiv:2112.02355*, 2021.
- [34] F. Fleuret *et al.*, “Test time adaptation through perturbation robustness,” in *Advances in Neural Information Processing Systems Workshop*, 2021.
- [35] Y. Iwasawa and Y. Matsuo, “Test-time classifier adjustment module for model-agnostic domain generalization,” in *Advances in Neural Information Processing Systems*, vol. 34, 2021.
- [36] Z. Li and D. Hoiem, “Learning without forgetting,” *IEEE transactions on pattern analysis and machine intelligence*, vol. 40, no. 12, pp. 2935–2947, 2017.
- [37] D. Rolnick, A. Ahuja, J. Schwarz, T. P. Lillicrap, and G. Wayne, “Experience replay for continual learning,” in *Advances in Neural Information Processing Systems*, 2019.
- [38] M. Farajtabar, N. Azizan, A. Mott, and A. Li, “Orthogonal gradient descent for continual learning,” in *International Conference on Artificial Intelligence and Statistics*, 2020, pp. 3762–3773.
- [39] S. Niu, J. Wu, Y. Zhang, Y. Guo, P. Zhao, J. Huang, and M. Tan, “Disturbance-immune weight sharing for neural architecture search,” *Neural Networks*, vol. 144, pp. 553–564, 2021.
- [40] S. Mittal, S. Galesso, and T. Brox, “Essentials for class incremental learning,” in *IEEE Conference on Computer Vision and Pattern Recognition*, June 2021, pp. 3513–3522.
- [41] Z. Pei, Z. Cao, M. Long, and J. Wang, “Multi-adversarial domain adaptation,” in *AAAI Conference on Artificial Intelligence*, 2018.
- [42] K. Saito, K. Watanabe, Y. Ushiku, and T. Harada, “Maximum classifier discrepancy for unsupervised domain adaptation,” in *IEEE Conference on Computer Vision and Pattern Recognition*, 2018, pp. 3723–3732.
- [43] Y. Zhang, Y. Wei, Q. Wu, P. Zhao, S. Niu, J. Huang, and M. Tan, “Collaborative unsupervised domain adaptation for medical image diagnosis,” *IEEE Transactions on Image Processing*, vol. 29, pp. 7834–7844, 2020.
- [44] Y. Zhang, S. Niu, Z. Qiu, Y. Wei, P. Zhao, J. Yao, J. Huang, Q. Wu, and M. Tan, “Covid-da: deep domain adaptation from typical pneumonia to covid-19,” *arXiv preprint arXiv:2005.01577*, 2020.
- [45] Z. Qiu, Y. Zhang, H. Lin, S. Niu, Y. Liu, Q. Du, and M. Tan, “Source-free domain adaptation via avatar prototype generation and adaptation,” in *International Joint Conference on Artificial Intelligence*, 2021.
- [46] J. Liang, D. Hu, and J. Feng, “Do we really need to access the source data? source hypothesis transfer for unsupervised domain adaptation,” in *International Conference on Machine Learning*, 2020, pp. 6028–6039.
- [47] C. Guo, G. Pleiss, Y. Sun, and K. Q. Weinberger, “On calibration of modern neural networks,” in *International conference on machine learning*. PMLR, 2017, pp. 1321–1330.
- [48] M. P. Naeini, G. Cooper, and M. Hauskrecht, “Obtaining well calibrated probabilities using bayesian binning,” in *Proceedings of the AAAI conference on artificial intelligence*, vol. 29, no. 1, 2015.
- [49] J. Zhang, B. Kailkhura, and T. Y.-J. Han, “Mix-n-match: Ensemble and compositional methods for uncertainty calibration in deep learning,” in *International conference on machine learning*. PMLR, 2020, pp. 11 117–11 128.
- [50] A. Kumar, S. Sarawagi, and U. Jain, “Trainable calibration measures for neural networks from kernel mean embeddings,” in *International Conference on Machine Learning*. PMLR, 2018, pp. 2805–2814.
- [51] S. Seo, P. H. Seo, and B. Han, “Learning for single-shot confidence calibration in deep neural networks through stochastic inferences,” in *Proceedings of the IEEE/CVF conference on computer vision and pattern recognition*, 2019, pp. 9030–9038.
- [52] S. Park, O. Bastani, J. Weimer, and I. Lee, “Calibrated prediction with covariate shift via unsupervised domain adaptation,” in *International Conference on Artificial Intelligence and Statistics*. PMLR, 2020, pp. 3219–3229.
- [53] X. Wang, M. Long, J. Wang, and M. Jordan, “Transferable calibration with lower bias and variance in domain adaptation,” *Advances in Neural Information Processing Systems*, vol. 33, pp. 19 212–19 223, 2020.
- [54] A. Karandikar, N. Cain, D. Tran, B. Lakshminarayanan, J. Shlens, M. C. Mozer, and B. Roelofs, “Soft calibration objectives for neural networks,” *Advances in Neural Information Processing Systems*, vol. 34, pp. 29 768–29 779, 2021.
- [55] H. S. Yoon, J. T. J. Tee, E. Yoon, S. Yoon, G. Kim, Y. Li, and C. D. Yoo, “ESD: Expected squared difference as a tuning-free trainable calibration measure,” in *International Conference on Learning Representations*, 2023.
- [56] W. Liu, X. Wang, J. Owens, and Y. Li, “Energy-based out-of-distribution detection,” in *Advances in Neural Information Processing Systems*, vol. 33, 2020.
- [57] C. Berger, M. Paschali, B. Glocker, and K. Kamnitsas, “Confidence-based out-of-distribution detection: A comparative study and analysis,” in *Uncertainty for Safe Utilization of Machine Learning in Medical Imaging, and Perinatal Imaging, Placental and Preterm Image Analysis*. Springer, 2021, pp. 122–132.
- [58] O. Chapelle and A. Zien, “Semi-supervised classification by low density separation,” in *International workshop on artificial intelligence and statistics*. PMLR, 2005, pp. 57–64.
- [59] J. Liang, R. He, and T. Tan, “A comprehensive survey on test-time adaptation under distribution shifts,” *arXiv preprint arXiv:2303.15361*, 2023.
- [60] Y. Gal and Z. Ghahramani, “Dropout as a bayesian approximation: Representing model uncertainty in deep learning,” in *international conference on machine learning*. PMLR, 2016, pp. 1050–1059.
- [61] G. Hinton, O. Vinyals, and J. Dean, “Distilling the knowledge in a neural network,” *arXiv preprint arXiv:1503.02531*, 2015.
- [62] C. Szegedy, V. Vanhoucke, S. Ioffe, J. Shlens, and Z. Wojna, “Rethinking the inception architecture for computer vision,” in *Proceedings of the IEEE conference on computer vision and pattern recognition*, 2016, pp. 2818–2826.
- [63] G. Huang, Y. Sun, Z. Liu, D. Sedra, and K. Q. Weinberger, “Deep networks with stochastic depth,” in *Computer Vision—ECCV 2016: 14th European Conference, Amsterdam, The Netherlands, October 11–14, 2016, Proceedings, Part IV 14*. Springer, 2016, pp. 646–661.
- [64] Q. Wang, O. Fink, L. Van Gool, and D. Dai, “Continual test-time domain adaptation,” in *Proceedings of the IEEE/CVF Conference on Computer Vision and Pattern Recognition*, 2022, pp. 7201–7211.
- [65] D. Hendrycks, S. Basart, N. Mu, S. Kadavath, F. Wang, E. Dorundo, R. Desai, T. Zhu, S. Parajuli, M. Guo *et al.*, “The many faces of robustness: A critical analysis of out-of-distribution generalization,” in *IEEE Conference on Computer Vision and Pattern Recognition*, 2021, pp. 8340–8349.
- [66] C. Sakaridis, D. Dai, and L. Van Gool, “ACDC: The adverse conditions dataset with correspondences for semantic driving scene understanding,” in *Proceedings of the IEEE/CVF International Conference on Computer Vision (ICCV)*, October 2021.
- [67] A. Dosovitskiy, L. Beyer, A. Kolesnikov, D. Weissenborn, X. Zhai, T. Unterthiner, M. Dehghani, M. Minderer, G. Heigold, S. Gelly *et al.*, “An image is worth 16x16 words: Transformers for image recognition at scale,” in *International Conference on Learning Representations*, 2021.
- [68] E. Xie, W. Wang, Z. Yu, A. Anandkumar, J. M. Alvarez, and P. Luo, “Segformer: Simple and efficient design for semantic segmentation with transformers,” *Advances in Neural Information Processing Systems*, vol. 34, pp. 12 077–12 090, 2021.
- [69] M. Cordts, M. Omran, S. Ramos, T. Rehfeld, M. Enzweiler, R. Benenson, U. Franke, S. Roth, and B. Schiele, “The cityscapes dataset for semantic

- urban scene understanding,” in *Proceedings of the IEEE conference on computer vision and pattern recognition*, 2016, pp. 3213–3223.
- [70] M. P. Naeini, G. Cooper, and M. Hauskrecht, “Obtaining well calibrated probabilities using bayesian binning,” in *Proceedings of the AAAI conference on artificial intelligence*, vol. 29, no. 1, 2015.
 - [71] H. Zhao, Y. Liu, A. Alahi, and T. Lin, “On pitfalls of test-time adaptation,” in *International Conference on Machine Learning (ICML)*, 2023.
 - [72] A. Krizhevsky, G. Hinton *et al.*, “Learning multiple layers of features from tiny images,” 2009.
 - [73] J. Deng, W. Dong, R. Socher, L.-J. Li, K. Li, and L. Fei-Fei, “Imagenet: A large-scale hierarchical image database,” in *IEEE Conference on Computer Vision and Pattern Recognition*, 2009, pp. 248–255.
 - [74] Y. Wang, H. Wang, Y. Shen, J. Fei, W. Li, G. Jin, L. Wu, R. Zhao, and X. Le, “Semi-supervised semantic segmentation using unreliable pseudo-labels,” in *Proceedings of the IEEE/CVF Conference on Computer Vision and Pattern Recognition*, 2022, pp. 4248–4257.
 - [75] T.-Y. Pan, C. Zhang, Y. Li, H. Hu, D. Xuan, S. Changpinyo, B. Gong, and W.-L. Chao, “On model calibration for long-tailed object detection and instance segmentation,” *Advances in Neural Information Processing Systems*, vol. 34, pp. 2529–2542, 2021.
 - [76] A. Ashukha, A. Lyzhov, D. Molchanov, and D. P. Vetrov, “Pitfalls of in-domain uncertainty estimation and ensembling in deep learning,” in *International Conference on Learning Representations*, 2020.
 - [77] E. Wong, L. Rice, and J. Z. Kolter, “Fast is better than free: Revisiting adversarial training,” in *International Conference on Learning Representations*, 2020.
 - [78] E. Rusak, L. Schott, R. S. Zimmermann, J. Bitterwolf, O. Bringmann, M. Bethge, and W. Brendel, “A simple way to make neural networks robust against diverse image corruptions,” in *European Conference on Computer Vision*, 2020, pp. 53–69.
 - [79] D. Madaan, J. Shin, and S. J. Hwang, “Learning to generate noise for multi-attack robustness,” in *International Conference on Machine Learning*, 2021, pp. 7279–7289.
 - [80] S. Lim, I. Kim, T. Kim, C. Kim, and S. Kim, “Fast autoaugment,” in *Advances in Neural Information Processing Systems*, vol. 32, 2019, pp. 6665–6675.
 - [81] D. Hendrycks, N. Mu, E. D. Cubuk, B. Zoph, J. Gilmer, and B. Lakshminarayanan, “Augmix: A simple data processing method to improve robustness and uncertainty,” in *International Conference on Learning Representations*, 2020.
 - [82] B. Li, F. Wu, S.-N. Lim, S. Belongie, and K. Q. Weinberger, “On feature normalization and data augmentation,” in *IEEE Conference on Computer Vision and Pattern Recognition*, 2021, pp. 12 383–12 392.
 - [83] H. Yao, Y. Wang, S. Li, L. Zhang, W. Liang, J. Zou, and C. Finn, “Improving out-of-distribution robustness via selective augmentation,” in *International Conference on Machine Learning*, 2022.
 - [84] D. Zhang, K. Ahuja, Y. Xu, Y. Wang, and A. Courville, “Can subnetwork structure be the key to out-of-distribution generalization?” in *International Conference on Machine Learning*, 2021, pp. 12 356–12 367.
 - [85] Y. Guo, D. Stutz, and B. Schiele, “Improving corruption and adversarial robustness by enhancing weak subnets,” *arXiv preprint arXiv:2201.12765*, 2022.

Supplementary Materials for “Uncertainty-Calibrated Test-Time Model Adaptation without Forgetting”

In the supplementary, we provide more implementation details and more experimental results of our EATA. We organize our supplementary as follows.

- In Section A, we provide more details of our proposed EATA and EATA-C.
- In Section B, we show more experimental results to compare the out-of-distribution performance, calibration and efficiency with state-of-the-art methods on ImageNet-C with different corruption types.
- In Section C, we give more experimental results to demonstrate the anti-forgetting ability of our EATA.
- In Section D, we provide more discussions on related training-time robustification studies.

APPENDIX A

MORE DETAILS OF EATA AND EATA-C

A.1 Overall Design of EATA

We provide an overview of our EATA. As shown in Figure A, given a trained base model f_{Θ^o} , we perform test-time adaptation with a model f_{Θ} that is initialized from Θ^o . During the adaptation process, we only update the parameters of batch normalization layers in f_{Θ} and froze the rest parameters. When a batch of test sample $\mathcal{X} = \{\mathbf{x}_b\}_{b=1}^B$ comes, we calculate a sample-adaptive weight $S(\mathbf{x})$ for each test sample to identify whether the sample is active for adaptation or not. We only perform backward propagation with the samples whose $S(\mathbf{x}) \neq 0$. Moreover, we propose an anti-forgetting regularizer to prevent the model parameters Θ changing too much from Θ^o .

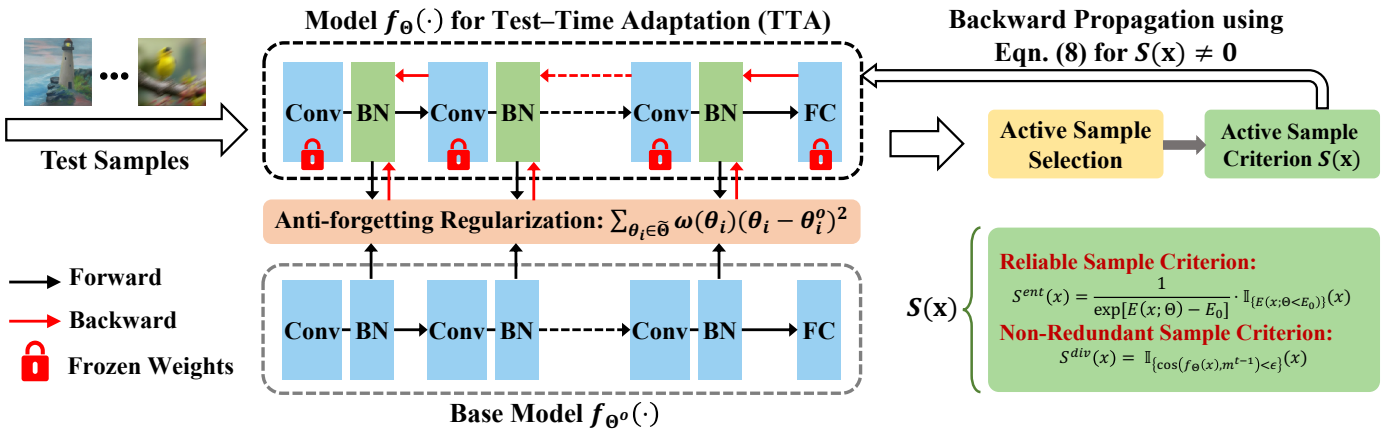


Fig. A. An illustration of the proposed EATA, which consists of a sample-efficient entropy minimization loss for test-time adaptation, and an anti-forgetting regularization to constrain important parameters from drastic change.

A.2 More Details on Datasets

Following the settings of Tent [12] and MEMO [14], we conduct experiments on four benchmark datasets for out-of-distribution generalization, *i.e.*, CIFAR-10-C, ImageNet-C [9], ImageNet-R [65], and ACDC [66].

CIFAR-10-C and **ImageNet-C** consist of corrupted versions of the validation images on CIFAR-10 [72] and ImageNet [73], respectively. The corruptions include 15 diverse types of 4 main categories (*i.e.*, noise, blur, weather, and digital). Each corruption type has 5 different levels of severity.

ImageNet-R contains 30,000 images with various artistic renditions of 200 ImageNet classes, which are primarily collected from Flickr and filtered by Amazon MTurk annotators.

ACDC contains four categories of images collected in adverse conditions, including fog, night, rain, and snow. Following [64], we use 400 unlabeled images from each adverse condition for adaptation.

A.3 More Experimental Protocols

Our EATA and EATA-C.

Following Tent [12] and CoTTA [64], we use ResNet-26 for CIFAR-10 experiments, ResNet-50 and ViTBase for ImageNet experiments, and Segformer-B5 for ACDC experiments. In classification experiments, the models are trained on the original CIFAR-10 or ImageNet training set and then tested on clean or the aforementioned OOD test sets. In semantic segmentation experiments, the model is

trained on Cityscapes and then tested on ACDC. For a fair comparison, the parameters of ViTBase and Segformer-B5 are directly obtained from the *timm*¹ and Segformer [68], respectively. ResNet-50 is trained via the official code in the *torchvision*² library with stochastic depth. ResNet-26 is trained via the official code of TTT by the same hyper-parameters, replacing the group norm with the batch norm, and removing the rotation head. For test time adaptation, we use SGD as the update rule, with a momentum of 0.9 and a batch size of 64. In EATA and ETA, the learning rate is set to 0.005 on CIFAR-10, 0.00025/0.001 for ResNet-50/ViTBase on ImageNet, and 7.5×10^{-5} on ACDC, respectively (following Tent, SAR and CoTTA). The entropy constant E_0 in Eqn. (3) is set to $0.4 \times \ln C$ in classification experiments and $0.1 \times \ln C$ in segmentation, where C is the number of task classes. The ϵ in Eqn. (6) is set to 0.4 for CIFAR-10, and 0.05 for ImageNet and ACDC. The trade-off parameter β in Eqn. (8) is set to 1/2,000/500 for CIFAR-10/ImageNet/ACDC to make two losses have a similar magnitude. In EATA-C, the learning rate is set to 0.005/0.1 for ResNet-50/ViTBase on ImageNet, and 0.0005 on ACDC, respectively. The sub-network is obtained via stochastic depth regularization [63] with a drop ratio of 0.2/0.6 for ImageNet/ACDC. The entropy constant E_0 in Eqn. (3) is set to $0.4/0.5 \times \ln C$, and the ϵ in Eqn. (6) is set to 0.05/0.07 for ViTBase/ResNet-50 on ImageNet. In Eqn. (14), the trade-off parameter α is set to 50/500 on ImageNet/ACDC and β is set to 0.1 on ImageNet. Note that for the semantic segmentation task, our EATA-C does not perform min-max entropy regularization and active sample selection due to the long-tailed problem [74], [75]. For both EATA and EATA-C, the moving average factor α in Eqn. (4) is set to 0.1, and we use 2,000/20 samples for ImageNet/ACDC to calculate $\omega(\theta_i)$ in Eqn. (9).

Compared Methods. For TTA [76], BN adaptation [32], MEMO [14], CoTTA [64], and SAR [18] the hyper-parameters follow their original papers or MEMO. Specifically, the augmentation size of TTA [76] is set to 32 and 64 for CIFAR-10 and ImageNet, respectively. For BN adaptation [32], both the batch size B and prior strength N are set to 64. The learning rate in CoTTA [64] for ViTBase is set to 0.005, and the augmentation threshold p_{th} is set to 0.1. Other hyper-parameter settings of CoTTA, and the hyper-parameter settings of MEMO [14] and SAR [18] can be found in their original paper. For Tent [12], we use SGD as the update rule with a momentum of 0.9. The batch size is 64 for both ImageNet and CIFAR-10 experiments. The learning rate is set to 0.00025/0.001 for ResNet-50/ViTBase on ImageNet and 0.005 on CIFAR-10, respectively. Note that the hyper-parameters of Tent are totally the same as our EATA for a fair comparison. For TTT [11], we strictly follow their original settings except for the augmentation size at test time for ImageNet experiments. According to TTT’s implementation, the augmentation size is set to 64, which, however, is very time-consuming (e.g., about 12 GPU hours on a single Tesla V100 GPU on ImageNet-C with a specific corruption type and severity level). In our implementation, we decrease this augmentation size to 20, which has only a slight performance difference compared with augmentation size 64. For example, the performances of TTT on ImageNet-C (Gaussian noise, severity level 5) with ResNet-18 are 26.2% (64) vs. 26.0% (20). We recommend the original papers of the above methods to readers for more implementation details.

APPENDIX B

MORE RESULTS ON OUT-OF-DISTRIBUTION PERFORMANCE, EFFICIENCY AND CALIBRATION

In Table D, we provide more results to compare our EATA and EATA-C with state-of-the-art methods in the single-domain adaptation scenario on ImageNet-C with the severity level 5. Although the compared methods exhibit stronger performance in the less challenging adaptation scenario, our EATA and EATA-C still demonstrate substantial superiority. Specifically, by filtering the unreliable and redundant samples from adaptation, our EATA achieves significant accuracy improvement while requiring less backward-propagation (e.g., 55.5% (72,446) vs. 61.8% (32,524) over the best method SAR on ViTBase). Meanwhile, EATA-C further enhances performance while mitigating calibration error on both ResNet-50 and ViTBase, verifying the promising effectiveness of our EATA and EATA-C across different adaptation scenarios.

In Table E, we provide the complete results for the lifelong test-time adaptation on ACDC. Compared with Tent, our EATA effectively alleviates error accumulation by excluding unreliable gradients and constraining important weights from drastic changes. Furthermore, besides maintaining strong performance in the long term, our EATA-C is able to further accumulate knowledge to improve performance over adaptation, demonstrating strong potential.

In Figure B, we show the number of backward propagation of our ETA on ImageNet-C with different corruption types and severity levels. Across various corruption types, our ETA shows great superiority over existing methods in terms of adaptation efficiency. Compared with MEMO ($50,000 \times 64$) and Tent (50,000), our ETA only requires 31,741 backward passes (averaged over 15 corruption types) when the severity level is set to 3. The reason is that we exclude some unreliable and redundant test samples out of test-time optimization. In this case, we only need to perform backward computation on those remaining test samples, leading to improved efficiency.

In Table F, we compared ETA and EATA with existing methods on CIFAR-10-C. Under the same base model (ResNet-26 with batch normalization), ETA achieves a lower average error than Tent (19.4% vs. 20.2%) with fewer requirements of back-propagation (8,192 vs. 10,000). Moreover, the performance gain over the base model of ETA is larger than that of TTT, i.e., +9.0% vs. +7.2% on accuracy. These results are consistent with the ones on ImageNet-C/R, further demonstrating the effectiveness and superiority of our method.

Comparison with Tent using Different Learning Rates. In our sample-adaptive weight $S(\mathbf{x})$ in Eqn. (6), each test sample has a specific weight $S(\mathbf{x})$ and the value of $S(\mathbf{x})$ is always larger than 1. In this sense, training with sample-adaptive weight $S(\mathbf{x})$ indeed has the same effect as training with larger learning rates. Therefore, we compare our EATA with the baseline (Tent) using different learning rates. We increase the learning rate from 2.5×10^{-4} (which is the default of Tent) to 25.0×10^{-4} and report results in Table A.

With the learning rate increasing from 2.5×10^{-4} to 10.0×10^{-4} , the error of Tent decreases from 45.3% to 43.9%, indicating that a larger learning rate may enhance the performance in some cases. However, when the learning rate becomes larger to 20.0×10^{-4} , the

1. <https://github.com/pprp/timm>

2. <https://github.com/pytorch/vision>

performance of Tent degrades. More critically, our EATA method outperforms Tent with varying learning rates. These results verify that simply enlarging the learning rate is not able to achieve competitive performance with our proposed sample-adaptive adaptation method, demonstrating our superiority.

TABLE A
Comparison with Tent under different learning rates ($\times 10^{-4}$) on ImageNet-C (Gaussian noise) regarding Error (%).

Severity	EATA (ours)		Tent [12]		
	$lr = 2.5$	$lr = 2.5$	$lr = 10.0$	$lr = 20.0$	$lr = 25.0$
Level 3	42.6	45.3	43.9	44.4	45.1
Level 5	65.0	71.6	72.2	83.6	87.1

EATA under Different Random Orders. Table B records EATA’s performance (mean & stdev.) on randomly shuffled test samples with 10 different random seeds (from 2020 to 2029). From the results, EATA performs consistently across different random orders, showing the stability of EATA.

TABLE B
The mean and stdev. of corruption accuracy (%) of EATA over 10 random orders, on ImageNet-C (level 5) with ResNet-50.

Gauss.	Shot	Impul.	Defoc.	Glass	Motion	Zoom	Avg.
34.9 \pm 0.2	36.9 \pm 0.1	35.8 \pm 0.2	33.6 \pm 0.3	33.3 \pm 0.2	47.2 \pm 0.3	52.7 \pm 0.1	35.8 \pm 0.2

EATA with Different Numbers of Test Samples. We investigate the effect of the total number of test samples (N) in EATA, where fewer samples are sampled from the entire test set. From Table C, EATA works well and consistently outperforms Tent counterpart, regardless of the number of test samples. Meanwhile, if there are many test samples, EATA would benefit more, *i.e.*, larger accuracy gain.

TABLE C
Comparison with Tent [12] w.r.t. corruption accuracy (%) with fewer (N) test samples on ImageNet-C (Gaussian noise, level 5) with ResNet-50.

Method	$N=256$	$N=512$	$N=1,024$	$N=2,048$	$N=4,096$	$N=10,000$
Tent	13.7	18.2	14.8	15.2	17.5	20.9
EATA	14.8	20.1	16.3	18.7	23.5	27.6

APPENDIX C MORE RESULTS ON PREVENT FORGETTING

In this section, we provide more results to demonstrate the effectiveness of our EATA in preventing forgetting. We report the comparison results of EATA (lifelong) *vs.* Tent (lifelong) and EATA *vs.* Tent in Figures C and D, respectively. In the lifelong adaptation scenario, Tent suffers more severe ID performance degradation than that of reset adaptation (*i.e.*, Figure D), showing that the more optimization steps, the more severe forgetting. Moreover, with the increase of the severity level, the ID clean accuracy degradation of Tent increases accordingly. This result indicates that the OOD adaptation with more severe distribution shifts will result in more severe forgetting. In contrast, our methods achieve higher OOD corruption accuracy and, meanwhile maintain the ID clean accuracy (competitive to the original accuracy that is tested before any OOD adaptation) in both two adaptation scenarios (reset and lifelong). These results are consistent with that in the main paper and further demonstrate the effectiveness of our proposed anti-forgetting weight regularization.

APPENDIX D MORE DISCUSSIONS ON RELATED TRAINING-TIME ROBUSTIFICATION

To defend against distribution shifts, many prior studies seek to enlarge the training data distribution to enable it to cover the possible shift that might be encountered at test time, such as adversarial training strategies [77], [78], [79], various data augmentation techniques [65], [80], [81], [82], [83] and searching/enhancing sub-networks of a deep model [84], [85]. However, it is hard to anticipate all possible test shifts at training time. In contrast, we seek to conquer this test distribution shift by directly learning from test data.

TABLE D

Comparison with state-of-the-art methods on ImageNet-C with the highest severity level 5 regarding **Corruption Accuracy(%, \uparrow)** and **Expected Calibration Error(%, \downarrow)**. “BN” and “LN” denote batch and layer normalization. All results are evaluated in the **single-domain adaptation scenario** (*i.e.*, the model parameters are reset before adapting to a new corruption type) except for MEMO [14]. We use * to denote episodic adaptation.

Model	Method	Metric	Noise				Blur				Weather				Digital				Average	
			Gauss.	Shot	Impul.	Defoc.	Glass	Motion	Zoom	Snow	Frost	Fog	Brit.	Contr.	Elastic	Pixel	JPEG	Avg.	# Forwards	# Backwards
R-50 (BN)	Source	Acc. ECE	1.8 16.6	3.0 16.1	1.7 15.9	18.2 1.8	10.1 10.7	13.4 10.7	20.8 14.7	14.0 25.3	22.1 12.9	21.9 16.7	58.7 2.3	5.3 6.7	17.6 22.9	22.1 10.5	37.5 6.0	17.88 12.64	50,000	0
	BN Adapt	Acc. ECE	15.8 1.1	16.7 0.8	15.3 1.0	18.7 3.0	19.3 1.3	29.8 0.8	41.7 3.4	35.8 1.1	35.0 1.0	50.5 5.4	65.9 1.4	18.1 7.6	49.3 4.3	51.7 3.8	42.0 4.8	33.70 2.72	50,000	0
	Tent	Acc. ECE	28.0 11.7	30.1 11.2	28.1 11.1	29.9 12.6	29.5 12.3	42.2 7.7	49.7 5.4	46.2 6.5	41.5 8.8	57.7 3.4	67.1 2.9	30.0 21.9	55.7 3.5	58.3 3.7	52.5 4.0	43.11 8.46	50,000	50,000
	MEMO*	Acc. ECE	6.8 24.1	8.5 24.2	7.5 22.9	20.5 5.3	13.4 19.3	19.8 14.8	25.8 23.4	22.1 30.4	27.7 18.7	27.6 24.6	60.9 7.2	11.3 14.9	24.4 29.4	32.2 19.3	37.9 13.6	23.09 19.47	50,000×65	50,000×64
	CoTTA	Acc. ECE	19.9 3.6	20.8 4.5	19.4 3.5	17.4 10.0	22.1 7.7	36.3 5.2	47.9 3.2	41.7 3.8	39.9 4.9	55.8 1.8	66.9 3.8	22.1 16.7	54.6 2.4	57.5 2.4	47.2 1.4	37.97 5.00	151,753	50,000
	SAR	Acc. ECE	29.6 3.7	31.9 4.0	28.3 3.3	30.5 7.4	30.5 6.9	43.2 3.2	50.3 1.7	47.3 1.8	43.2 2.9	58.3 1.3	67.2 1.6	38.4 8.7	55.7 1.3	58.6 1.3	53.2 1.3	44.42 3.37	78,661	52,660
	EATA (Ours)	Acc. ECE	35.6 10.5	37.8 10.2	36.1 10.3	35.3 12.9	35.4 12.3	47.6 8.3	53.1 6.6	51.4 6.7	45.9 8.2	60.1 4.7	67.6 4.5	45.8 9.9	58.2 5.1	60.3 5.3	55.4 5.6	48.36 8.08	50,000	26,188
	EATA-C (Ours)	Acc. ECE	37.2 7.1	39.2 6.8	38.0 6.8	35.5 9.3	35.9 8.9	48.2 4.3	52.3 3.6	51.9 3.0	46.5 4.5	60.4 1.8	67.3 1.9	48.7 4.5	58.0 2.3	60.5 2.4	56.0 2.4	49.04 4.63	82,492	32,492
ViT (LN)	Source	Acc. ECE	12.9 14.2	17.6 11.3	11.7 15.2	34.4 2.2	27.7 8.2	43.7 6.0	36.2 10.7	43.4 7.5	45.4 8.3	52.8 5.0	73.3 2.1	45.5 2.3	37.9 12.2	54.7 4.1	60.2 2.9	39.84 7.48	50,000	0
	Tent	Acc. ECE	33.4 24.1	42.1 10.1	41.4 11.7	48.8 8.6	45.2 10.4	54.9 7.5	48.2 12.4	55.6 8.0	55.1 8.0	64.4 4.8	75.2 2.4	62.5 5.2	51.6 10.0	65.5 4.3	65.0 4.1	53.92 8.78	50,000	50,000
	MEMO*	Acc. ECE	32.2 33.0	35.1 32.5	32.6 33.2	37.5 36.7	28.5 45.7	43.3 41.0	40.1 47.2	45.2 39.8	47.0 38.8	53.9 33.7	73.3 20.0	53.3 26.7	39.6 48.5	59.5 30.4	62.8 27.2	45.60 35.63	50,000×65	50,000×64
	CoTTA	Acc. ECE	45.6 9.0	46.8 8.9	28.1 9.9	45.3 7.9	42.0 12.9	57.6 8.1	49.8 12.1	59.5 7.1	57.6 9.0	65.2 6.4	74.9 4.3	58.2 6.6	55.5 10.7	66.3 6.7	65.7 6.6	54.54 8.42	50,000×3	50,000
	SAR	Acc. ECE	43.1 8.0	44.0 7.0	44.3 7.6	50.4 6.1	48.2 6.7	55.1 5.9	49.0 9.2	56.9 5.5	56.0 5.9	64.7 3.6	75.3 2.1	62.4 4.0	53.5 7.2	65.3 3.6	64.9 3.4	55.53 5.71	86,684	72,446
	EATA (Ours)	Acc. ECE	50.5 10.6	51.3 10.1	51.3 10.3	55.9 9.4	56.0 8.8	60.7 7.8	58.0 9.1	64.2 6.4	62.2 7.3	70.1 5.4	77.4 2.8	66.7 6.1	63.9 6.6	70.5 4.5	68.9 4.8	61.84 7.34	50,000	32,524
	EATA-C (Ours)	Acc. ECE	56.6 5.3	57.6 4.8	57.2 5.2	57.8 5.3	59.8 4.1	64.6 3.5	64.4 4.0	69.1 2.8	67.2 2.7	73.3 2.1	78.6 1.4	67.0 2.9	70.2 2.2	73.9 1.7	71.2 2.2	65.90 3.34	82,364	32,364

TABLE E

Semantic segmentation results (mIoU in %) on the Cityscapes-to-ACDC in lifelong test-time adaptation scenario. The model is continually adapted to the four adverse conditions for ten rounds without resetting model parameters, *i.e.*, **lifelong adaptation**. All results are evaluated based on the Segformer-B5 model.

Condition	Fog	Night	Rain	Snow	Fog	Night	Rain	Snow	Fog	Night	Rain	Snow	Fog	Night	Rain	Snow	Fog	Night	Rain	Snow	cont.
Round	1				2				3				4				5				cont.
Source	69.1	40.3	59.7	57.8	69.1	40.3	59.7	57.8	69.1	40.3	59.7	57.8	69.1	40.3	59.7	57.8	69.1	40.3	59.7	57.8	cont.
BN Stats Adapt	62.3	38.0	54.6	53.0	62.3	38.0	54.6	53.0	62.3	38.0	54.6	53.0	62.3	38.0	54.6	53.0	62.3	38.0	54.6	53.0	cont.
TENT-continual	69.0	40.2	60.0	57.3	68.4	39.1	60.0	56.4	67.6	37.9	59.7	55.3	66.6	36.6	58.9	54.2	65.9	35.3	57.9	53.3	cont.
CoTTA	70.9	41.1	62.4	59.7	70.9	41.0	62.5	59.7	70.9	40.8	62.6	59.7	70.8	40.6	62.6	59.7	70.8	40.6	62.6	59.7	cont.
EATA	69.1	40.5	59.8	58.1	69.3	41.1	60.0	58.4	69.3	41.5	60.1	58.6	69.3	41.8	60.1	58.6	69.2	42.1	59.9	58.5	cont.
EATA-C	71.0	44.3	63.1	61.1	71.9	44.7	63.9	62.5	72.0	46.1	64.2	63.1	72.0	47.3	64.9	63.8	71.8	46.2	64.3	64.0	cont.
Round	6				7				8				9				10				Mean
Source	69.1	40.3	59.7	57.8	69.1	40.3	59.7	57.8	69.1	40.3	59.7	57.8	69.1	40.3	59.7	57.8	69.1	40.3	59.7	57.8	56.7
BN Stats Adapt	62.3	38.0	54.6	53.0	62.3	38.0	54.6	53.0	62.3	38.0	54.6	53.0	62.3	38.0	54.6	53.0	62.3	38.0	54.6	53.0	52.0
TENT-continual	65.2	34.3	56.9	52.4	64.6	33.4	55.9	51.6	63.9	32.4	54.7	50.6	63.2	31.5	53.7	49.6	62.7	30.4	52.6	48.7	52.4
CoTTA	65.2	34.3	56.9	52.4	64.6	33.4	55.9	51.6	63.9	32.4	54.7	50.6	63.2	31.5	53.7	49.6	62.7	30.4	52.6	48.7	58.4
EATA	69.0	42.3	59.7	58.2	68.8	42.5	59.4	57.9	68.6	42.7	58.9	57.4	68.3	42.8	58.4	56.9	67.9	42.8	57.7	56.3	57.0
EATA-C	72.7	47.2	64.5	63.9	71.8	48.2	64.2	64.2	71.5	48.1	64.6	64.6	71.8	48.4	64.5	64.4	72.0	48.7	64.3	64.1	61.6

TABLE F

Comparison on CIFAR-10-C. Results are evaluated in the single-domain adaptation scenario, and averaged over 15 different corruption types and 5 severity levels (totally 75). We use * to denote episodic adaptation.

Model	Acc. (%)	#Forwards	#Backwards
ResNet-26 (GroupNorm)	77.5	10,000	0
• TTA [76]	80.1 _(+2.6)	10,000×32	0
• MEMO* [14]	80.4 _(+2.9)	10,000×33	10,000×32
ResNet-26 (GroupNorm)+JT	77.2	10,000	0
• TTT [11]	84.4 _(+7.2)	10,000×33	10,000×32
• TTT*	78.5 _(+1.3)	10,000×33	10,000×32
ResNet-26 (BatchNorm)	71.6	10,000	0
• Tent [12]	79.8 _(+8.2)	10,000	10,000
• ETA (Ours)	80.6 _(+9.0)	10,000	8,192
• EATA (Ours)	80.3 _(+8.7)	10,000	8,153

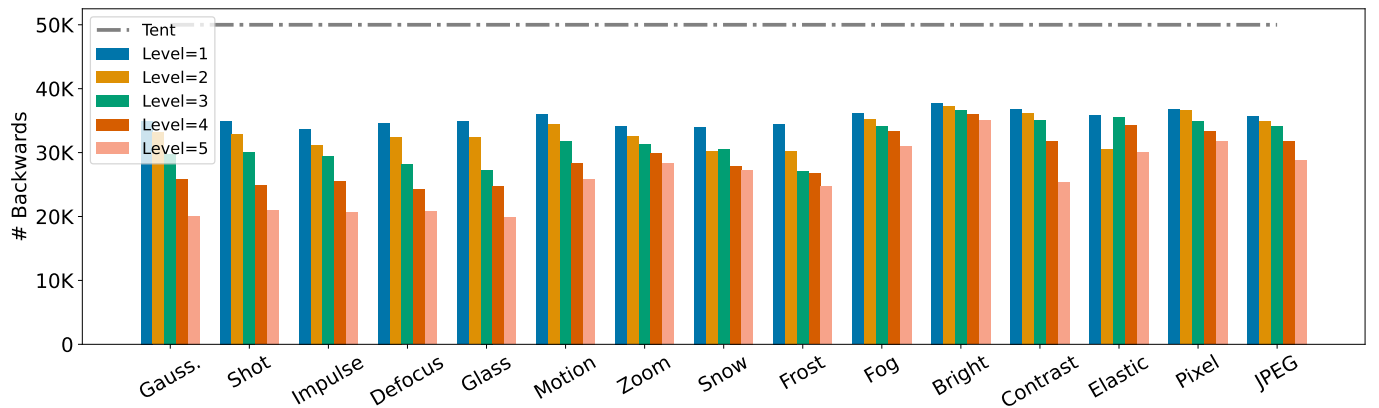


Fig. B. Comparison between ETA and Tent in terms of the number of backward propagation on ImageNet-C with different corruption types and severity levels.

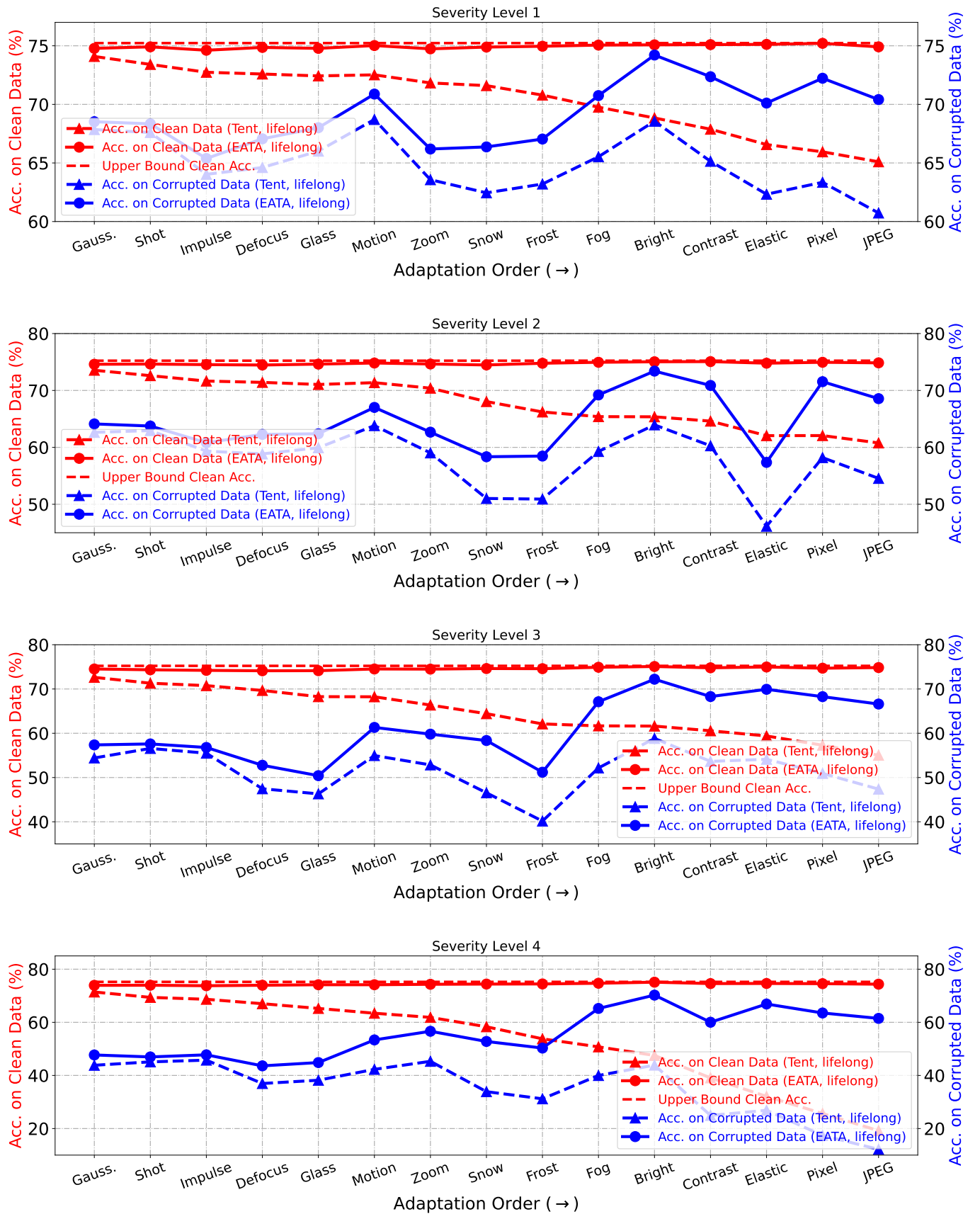


Fig. C. Comparison of preventing forgetting on ImageNet-C (severity levels 1-4) with ResNet-50. We record the OOD corruption accuracy on each corrupted test set and the associated ID clean accuracy (after OOD adaptation). The model performs lifelong adaptation, in which the model parameters will never be reset.

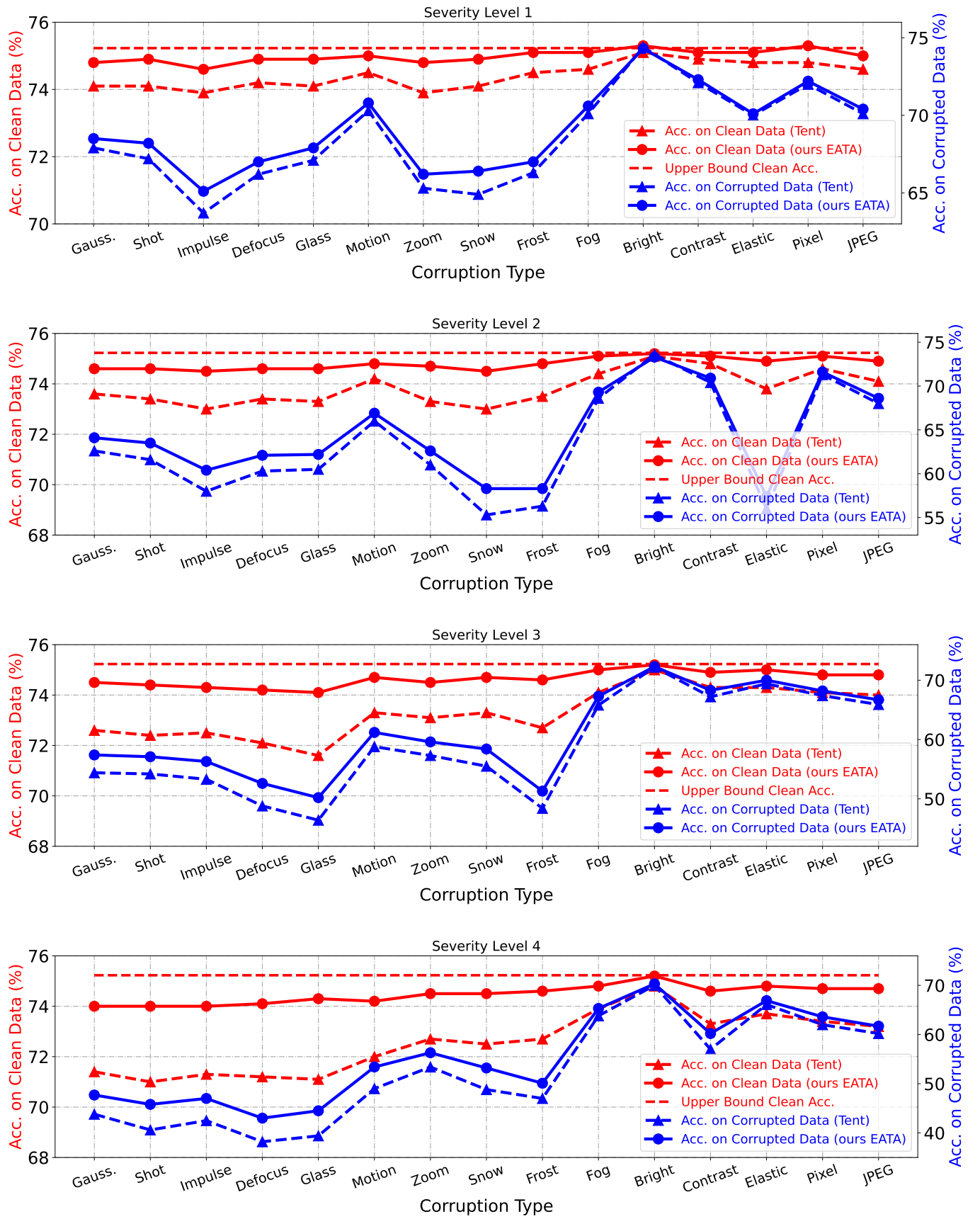


Fig. D. Comparisons of preventing forgetting on ImageNet-C (severity levels 1-4) with ResNet-50. We record the OOD corruption accuracy on each corrupted test set and the associated ID clean accuracy (after OOD adaptation). The model parameters of both Tent and our EATA are reset before adapting to a new corruption type.